IEEE Access
Multidisciplinary | Rapid Review | Open Access Journal

Received August 26, 2021, accepted September 29, 2021, date of publication October 4, 2021, date of current version October 12, 2021.

Digital Object Identifier 10.1109/ACCESS.2021.3117445

Highly Reliable Metro-Access Network Based on a Dual-Fiber Ring Architecture and Optimized Protection Mechanisms

ZERUI SONG[1,2], WEI JI[1,2], RUI YIN[2], JINGYAO LI[1,2], ZISU GONG[1,2], AND HAO YUN[1,2]

[1]Laboratory of Intelligent Communications and Multimedia Information Processing, Shandong University, Qingdao 266237, China
[2]School of Information Science and Engineering, Shandong University, Qingdao 266237, China

Corresponding authors: Wei Ji (jiwww@sdu.edu.cn) and Rui Yin (yinrui@sdu.edu.cn)

This work was supported in part by the National Natural Science Foundation of China under Grant 61571273 and Grant 61771292, in part by the National Key Research and Development Program of China under Grant 2017YFC0803403, in part by the Natural Science Foundation of Shandong Province of China under Grant ZR2016FM29, and in part by the Fundamental Research Funds of Shandong University.

ABSTRACT Network reliability is very important for the next generation of optical networks. In this paper, a highly reliable protection mechanism, which integrates the approaches of optical protection and microwave protection, is proposed for metro-access optical networks based on the wavelength division multiplexing (WDM) technique. By designing a scheme for the convergence of optical and wireless access and cooperating with designed remote nodes (RNs), not only can access for both wired and wireless service be provided simultaneously in each optical network unit (ONU) but also microwave protection can be realized when a failure occurs in a distribution segment. By developing a novel optical switch module (OSM) to cooperate with the dual-fiber ring structure, flexible switching can be achieved to protect against multiple types of failures in the feeder segment, including single-fiber faults, dual-fiber faults and multifiber faults. Based on the above structure, the influence of Rayleigh backscattering (RB) noise can be mitigated when the network is operating under all operating scenarios except for an inner-fiber fault. To further mitigate the influence of noise, optimization for upstream transmission performance is implemented by configuring a reflective semiconductor optical amplifier (RSOA). Furthermore, the feasibility of the overall scheme is verified through experiments and simulations under different operating conditions. The results show that the proposed mechanisms can achieve acceptable bit error rate performance and quality of service (QoS) metrics while also offering various advantages, including high reliability, large scale, and a relatively low cost.

INDEX TERMS Fiber fault, metro-access optical network, reliability, protection, wavelength division multiplexing (WDM).

I. INTRODUCTION

The explosive growth in internet traffic has heightened the need for developing next-generation optical network architecture [1]. Of particular promising and significant consideration is the metro-access optical network, which allows the number of central office (CO) sites per service area to be reduced by combining the characteristics of both metro and access networks in a single network. In this way, not only can the hierarchical telecom network architecture be simplified, but the operational complexity and cost are also reduced [1]–[3]. However, with the rapidly growing traffic and the current trend of CO consolidation, significant losses of data and service interruptions are becoming more likely with the occurrence of network faults [4], [5]. Hence, one of the most significant current concerns in developing next-generation optical network architecture is network reliability, and effective protection mechanisms are a key component for a highly reliable network architecture [6], [7].

To guarantee network reliability, in recent years, there has been an increasing amount of literature on resilient network architectures supporting failure recovery. For convenience, we review each scheme from two perspectives: the protection of the feeder section and the protection of the distribution section. It is important to note that whether the protection of the full path between the CO and the user is supported

The associate editor coordinating the review of this manuscript and approving it for publication was Thanh Ngoc Dinh.

may vary among the different types of demand scenarios because of the tradeoff between the reliability performance and investment cost [8]. The many protection schemes developed in attempting to resist different types of network failures are roughly divided into two groups. The first group is the mechanisms based on pure optical protection, which improve network reliability performance by adding redundant components and systems or developing cost-efficient architectures. There now exists a vast body of literature [9]–[13] on architectures supporting the protection of distribution sections for wavelength division multiplexing (WDM) passive optical networks (PONs) and hybrid time and wavelength division multiplexing (TWDM)-PONs. All of these schemes are based on a similar principle of utilizing the wavelength routing properties of arrayed waveguide grating (AWG) [9]–[11] or the power sharing properties of a splitter [12], [13] to select among a certain number of optical network units (ONUs) connected to each other to form a protective ring against distribution-fiber faults. Although these approaches could further improve network reliability, the existing literature on the protection of the distribution section fails to consider the possible situation that when there are more than two faults in such a protective ring, the above schemes can lead to a degradation in optical transmission performance, and all ONUs belonging to the same protective ring may even cease working, which will cause unfair failure risk sharing. Moreover, if a small number of ONUs are connected by a protective ring, especially in a relatively small-scale network, the cost sharing could be low.

On the other hand, network reliability of four nines or more cannot be achieved if the full path between the CO and the user is not protected [14]. Therefore, a large and growing body of literature [9]–[13], [15], [16] supporting the protection of the feeder segment concurrently has investigated satisfying the higher reliability requirement of the next-generation optical network. Overall, these schemes focus on the similar aim of developing cost-efficient architecture based on various physical topologies to resist network failures, such as the tree topology [9]–[11], single-fiber ring topology [13], [16], and dual-fiber ring topology [12], [15]. Among them, the schemes in [12] and [15], based on the dual-fiber ring architecture, can enable flexible switching, thus providing resistance against more types of faults on the feeder segment compared to a tree or single-fiber ring architecture [17], [16]. In these schemes, the complicated optical switch module (OSM) plays a vital role in the protection of the feeder segment. However, much of the design of complex OSMs thus far has been merely descriptive in nature, rather than based on the development of practical engineering, and it thus lacks the realistic parameters regarding OSMs obtained from tests such as the return loss, crosstalk and switching time, which are critical for demonstrating the feasibility of a scheme. Furthermore, some proposed architectures [11], [13], [16] support wavelength remodulation schemes based on reflective semiconductor optical amplifiers (RSOAs) to enhance the wavelength efficiency and achieve colorless ONU, which could be a cost-effective scheme because of the decrease of the construction cost for each ONU and the increase of the usage efficiency of each optical channel. However, the mitigation of Rayleigh backscattering (RB) noise has failed to be considered, which is the dominant factor limiting upstream transmission in an optical network with reflective ONUs [18]–[20]. In addition, none of these schemes perform systematic optimization for upstream transmission performance.

Another group is the approaches based on wireless protection [21]–[30], which reroute the traffic affected by failure to dedicated ONUs through wireless relay equipment and wireless links instead of expensive additional fiber deployment. One of the most promising access solutions for local and metropolitan areas is the wireless-optical broadband access network (WOBAN) architecture, as an optimal combination of an optical backhaul and wireless front-end, which contribute to a good scalable, cost effective, configurable and flexible communication system [31], [32]. Therefore, a great deal of previous research into survivable WOBAN architecture has focused on two aspects: the optimal deployment of survivable WOBANs [21]–[23], e.g., wireless router placement and backup radio configuration, and the design of survivable routing-based algorithms [24], [25]. Furthermore, from the perspective of reliability, compared to the aforementioned pure optical protection scheme, although the above studies can provide more flexible protection to significantly enhance network reliability with a low deployment cost through a front-end wireless mesh network (WMN) [26], [31], they still suffer from two limitations. First, these schemes cannot be applied in the recovery of large-capacity fault scenarios, such as the protection of the feeder segment and even the protection of the distribution section of WDM networks due to the extremely high requirement of spare capacity for the backup segment. Second, the affected traffic via wireless routers may suffer from severe delays if multiple hops are experienced [17].

To address the above two disadvantages, as a promising candidate for large-capacity wireless access scenarios, although the development of survivable WOBAN architectures based on microwave or millimeter-wave (mmWave) techniques has been discussed extensively in the existing literature, most are restricted to focusing only on single protection techniques, e.g., wireless protection for the front end [27], [28] or pure optical protection for the backhaul [33], [34]. Thus far, very little research has been carried out on integrating optical and microwave or mmWave protection to provide more effective and flexible protection, and thus, these existing survivability studies also feature some of the unavoidable aforementioned defects belonging to a certain group of protection method. In one such study [29], Aldaya *et al.* presented a scheme focusing on protecting the feeder segment of time division multiplexed (TDM)-PONs, which was achieved by a photonic mmWave bridge architecture. The proposed photonic mmWave bridge is capable of converting baseband signals of 2.5 Gbit/s and 10 Gbit/s up to

the mmWave band and achieving wireless transmission over some distance. However, in contrast to microwave protection, despite mmWave protection seeming to tolerate faults with larger capacity, the connectivity and coverage of mmWave networks are limited by blockage problems due to their limited diffraction ability [35]–[38]. In another study [30], Yang *et al.* proposed a flexible PON architecture, which utilizes microwave connections to implement the backup in the distribution part of the network and to achieve cost-effective protection according to different reliability requirements. While integrated optical and microwave protection was adopted in their scheme, the protection of the feeder part was achieved by duplicating only the backup fiber, which cannot recover from the potential fault in which there are two broken fibers in the feeder part simultaneously. Furthermore, the network scale depends heavily on the stages of the cascaded AWGs due to its tree topology. Nevertheless, multiple stages of cascaded AWGs can cause the degradation of the optical transmission performance, especially for the scheme in which two wavelengths are set in one data channel of the AWG, which may in turn limit the distance between the CO and ONUs.

The focus of this study is to propose a highly reliable protection mechanism, which applies to metro-access networks based on the WDM technique, and to effectively address the aforementioned deficiencies. The specific contributions are as follows:

1) By integrating the approach of optical protection and microwave protection, the proposed protection mechanism can significantly improve network reliability without losing cost-effectiveness. This protection mechanism can meet the requirement of failure recovery in large-capacity communication scenarios, particularly for metro-access optical networks based on the WDM technique.
2) We develop an OSM based on realistic components and apply it to ensure the protection of the feeder segment, which can cooperate with the dual-fiber ring structure to defend the feeder segment against multiple failures, including single-fiber faults, dual-fiber faults and multifiber faults. Moreover, the OSM scheme can not only apply to practical engineering development but can also be upgraded easily and thus satisfy the low latency requirement of future high-speed optical networks.
3) Moreover, to enable the proposed mechanisms to be cost effective, we utilize a radio over fiber (RoF) transmission scheme based on optical carrier suppression (OCS) to cotransmit radio signals and baseband signals, which can not only avoid the usage of an up-converter in each ONU but can also simultaneously provide wired and wireless service for each ONU. As the microwave protection utilizes only the existing device for wireless access, no extra deployment cost needs to be introduced for the protection of the distribution segment.

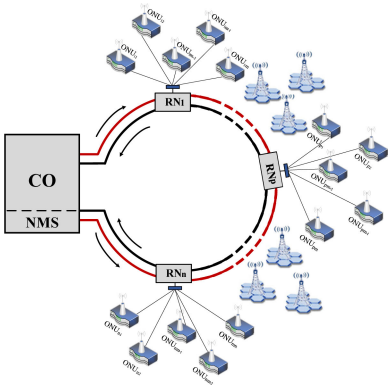

FIGURE 1. Schematic of the proposed dual-fiber ring architecture supporting multifault protection.

4) The influence of RB noise is mitigated in all the operating scenarios except for the inner-fiber fault. To mitigate the influence of noise, we discuss the process of improving the upstream transmission performance in multiple operating scenarios by configurating the optimal bias current of the RSOA.
5) The feasibility of the proposed scheme is very high, and this was analyzed comprehensively in terms of the network scale, network reliability, transmission performance and quality of service (QoS). The actual performance indicators of the OSM obtained in the experiments were applied to the above analysis, which enhances the reliability of the results.

The rest of this paper is organized as follows: In section II, the network architecture and operating principle under normal conditions are explained. In section III, three failure scenarios and the corresponding protection mechanisms are described in detail. In section IV, the scheme of bandwidth allocation in various operating scenarios is illustrated. The performance of the proposed scheme is analyzed in section V. Finally, we discuss and conclude the paper in section VI.

II. ARCHITECTURAL CONFIGURATION AND OPERATING PRINCIPLE

A. NETWORK ARCHITECTURE

The proposed network architecture that supports protection against multiple faults is shown in Fig. 1. It consists of a dual-fiber ring network and a star network, which are also called the dual-fiber ring section and the star section, respectively. Both the dual-fiber ring section and the star section are WDM networks. Moreover, the star section is a PON. In the dual-fiber ring section, a certain number of base stations (BSs) are deployed between two neighboring remote nodes (RNs) to form microwave connections. In the star section, m ONUs associated with the same RN occupy different wavelengths by means of WDM technology. It should be noted that the number of ONUs connected to each RN depends on various characteristics of the actual situation, such as the number of users in the region. However, for convenience of description,

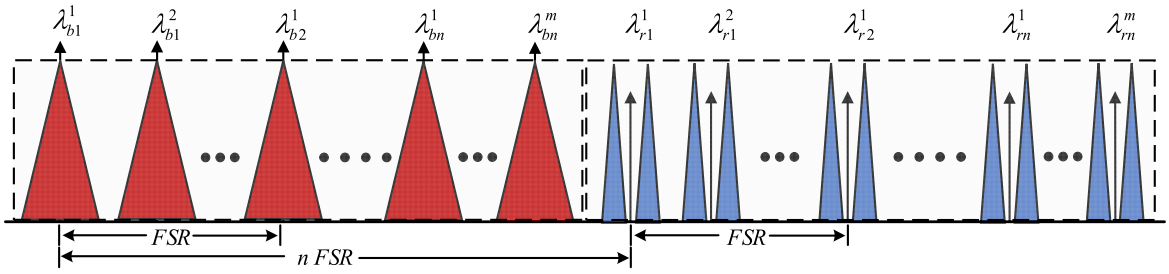

FIGURE 2. Schematic of wavelength assignment in this network.

suppose that there are n RNs and one CO in the dual-fiber ring and that each RN is connected to m ONUs in the proposed architecture. Hence, the network can accommodate $n \times m$ ONUs in total. When the network is operating, the dual-fiber ring section will be divided into two branches by a splitter, namely, an upper branch (CO-RN_1- RN_p) and a lower branch (CO-RN_n-RN_{n-p}), where $0 < p \leq n$. In cooperation with the OSM working in the corresponding mode, the downstream signals from transmitters propagate on the outer ring, while the upstream signals propagate on the inner ring before being injected into receivers by couplers. The operating principle of the OSM will be described in detail in the next subsection.

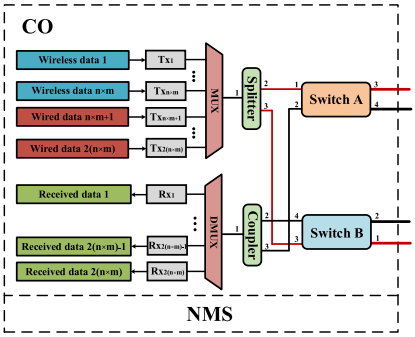

FIGURE 3. Schematic of the CO.

B. OPERATING PRINCIPLE

In the proposed scheme, two kinds of signals are supported by the network: baseband signals and radio signals. The baseband signals from the wired service and the radio signals from the wireless service together constitute the downstream signals. The specific assignment of the wavelengths for the signals of each kind in this network is shown in Fig. 2. In total, $n \times m$ wavelengths ($\lambda_{b1}^{1} \ldots \lambda_{bn}^{m}$) located in the red band are used to transmit baseband signals, and $n \times m$ wavelengths ($\lambda_{r1}^{1} \ldots \lambda_{rn}^{m}$) located in the blue band are used to transmit radio signals. Moreover, the optical carriers of the upstream signals originate from the downstream signals. Consider ONU_j^i ($0 < i \leq m, 0 < j \leq n$) connected to RN_j as an example. There are two wavelengths (λ_{bj}^{i} and λ_{rj}^{i}) allocated to this ONU, which are separated by n times the free spectral range (FSR), whereas the wavelengths of adjacent RNs are separated by one FSR.

The structure of the CO is depicted in Fig. 3. It contains one wavelength division multiplexer (MUX), one wavelength division demultiplexer (DMUX), one splitter, one coupler, one switch A, one switch B, $2(n \times m)$ transmitters (Tx), $2(n \times m)$ receivers (Rx), and one network management system (NMS) for responding to monitoring information in real time and configuring the entire network.

In the CO, there are two kinds of data that can be provided to users, referred to as wireless data and wired data, to simultaneously meet the coverage requirements for wireless and wired service. Radio signals are generated by employing an OCS scheme to realize wireless access and protection in the microwave band. This scheme possesses many advantages, including high receiver sensitivity; low spectral occupancy; low bandwidth requirements for radio frequency (RF) signals, electrical amplifiers (EAs), and optical modulators; and minimal power penalties over long delivery distances [39].

A schematic of the OSM is shown in Fig. 4. The OSM adopted in the ring network consists of two subsystems called switch A and switch B, which are installed alternately on the dual-fiber ring to achieve real-time switching for resistance against multiple faults in the ring network. Switch A and switch B each contain one 1×2 optical switch (OS), one full 2×2 OS, two dual full 2×2 OSs, and two 3-port circulators. However, the optical connections between them are different. Switch A and switch B are connected through an outer fiber connecting OS1 and OS3 and an inner fiber connecting OS2 and OS4 in the ring architecture. The outer fiber and the inner fiber are depicted in Fig. 4 as a red line and a black line, respectively.

Each of the OSs in the network has two possible states, called state 1 and state 2. The optical paths of each OS corresponding to state 1 and state 2 are depicted using red dotted lines and blue solid lines, respectively. The corresponding working states of the OSM in various modes are summarized in Table 1. There are three working modes of the OSM, corresponding to three operating scenarios in the ring network. In each working mode of the OSM, the downstream signals propagating in the upper branch of the ring network are always input through port 1 of switch A and output through port 3 of switch B, and the upstream signals are always input through port 4 of switch B and output through port 2 of switch A. By contrast, the downstream signals propagating in the lower branch of the ring network are always input through

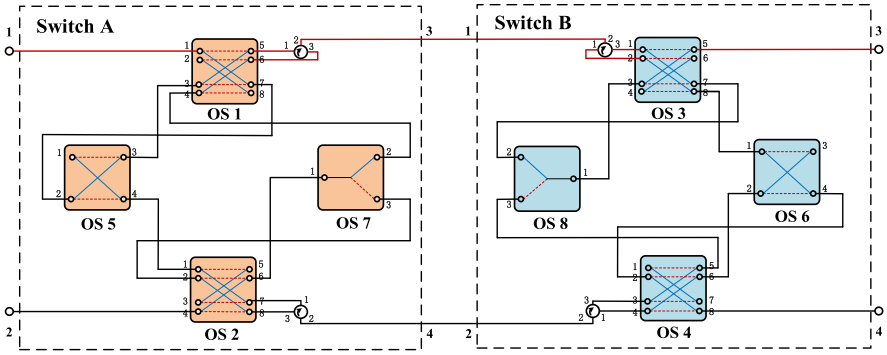

FIGURE 4. Schematic of the OSM.

TABLE 1. Working states of each OS in the OSM.

Mode	Switch state							
	Switch B				Switch A			
	OS 1	OS 2	OS 5	OS 7	OS 3	OS 4	OS 6	OS 8
1	state 1	state 1	state 1	state 2	state 1	state 1	state 2	state 1
2	state 2	state 2	state 2	state 2	state 2	state 2	state 2	state 2
3	state 2	state 2	state 1	state 1	state 2	state 2	state 1	state 1

port 3 of switch B and output through port 1 of switch A, and the upstream signals are always input through port 2 of switch A and output through port 4 of switch B. In this way, normal transmission of the downstream and upstream signals between adjacent RNs can be maintained even if a fault occurs in one of the ring fibers. The operating principle in each of the three working modes will be explained in detail in section III.

In this section, we discuss only the operations of the network under normal conditions. The operating principles for the other operating scenarios will be described in detail in section III. Here, RN_j $(0 < j \leq p)$ and RN_k $(n\text{-}p < k \leq n)$ are taken as an example to illustrate the operating principle of the network. When the network is operating in the normal scenario, the OSM will remain in working mode 1, as described in Table 1. In this case, the downstream signals output from port 2 of the splitter in the upper branch of the outer ring will be input through port 1 of switch A and then output through port 3 of switch A and will then propagate to RN_j in the clockwise direction, whereas the upstream signals transmitted from RN_j to the CO will travel in the opposite direction in the inner ring. In the lower branch of the outer ring, the downstream signals output from port 3 of the splitter will be input through port 3 of switch B and output through port 1 of switch B and will then propagate to RN_k in the counterclockwise direction, whereas the upstream signals coming from RN_k will similarly be transmitted to the CO in the opposite direction in the inner ring. In this way, since the upstream and downstream signals propagate in different fibers, the influence of RB caused by backpropagation between signals can be mitigated.

A schematic of an RN is depicted in Fig. 5. This RN consists of one switch A, one switch B, one AWG, one circulator, two erbium-doped fiber amplifiers (EDFAs), three couplers, three tunable fiber Bragg gratings (FBGs), two wavelength selectors (WSs), and four OSs. Note that not all RNs require EDFAs because the number of required EDFAs is determined by the scale of the network. In the RN, OS9 and OS10, with two possible working states, are used to change the directions of propagation of the downstream and upstream signals in the ring network. Both OS9 and OS10 are in working state 1 in the upper branch of the ring network and are in working state 2 in the lower branch. Therefore, when the downstream signals in the upper branch of the ring network enter port 1 of switch B in RN_j, they will pass through OS9 and then be amplified by EDFA1. Because both OS11 and OS12 are operating in state 1, the downstream signals output from EDFA1 will reach port 1 of WS1. According to the wavelength allocation scheme, some of the wavelengths $(\lambda^1_{bj} \ldots \lambda^m_{bj}, \lambda^1_{rj} \ldots \lambda^m_{rj})$ are output from port 2 of WS1, and the remaining wavelengths $(\lambda^1_{b(j+1)} \ldots \lambda^m_{bp}, \lambda^1_{r(j+1)} \ldots \lambda^m_{rp})$ are output from port 3 of WS1. After coupling by coupler 3, because their wavelengths are not the same as the wavelength reflected by FBG1, the downstream signals output from port 2 of WS1 will pass through FBG1, circulator 1 and the AWG in sequence. Then, the downstream signals demultiplexed by the AWG will be transmitted to the target ONU connected to RN_j through the distribution fiber between ONU^i_j and RN_j. The remaining wavelengths output from port 3 of WS1 will be coupled with the upstream signals coming from the ONUs connected to RN_j by coupler 1 and will next pass through port 1 and port 3 of switch A, finally reaching RN_{j+1} through the outer

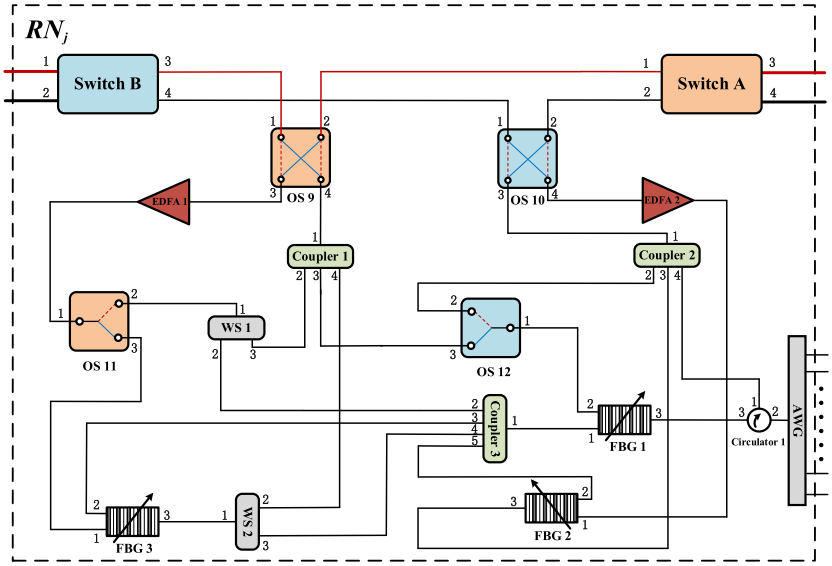

FIGURE 5. Schematic of an RN.

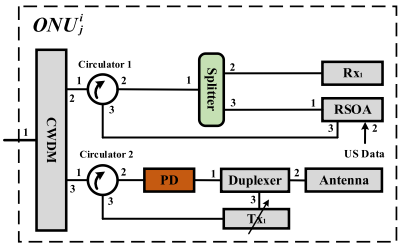

FIGURE 6. Schematic of an ONU.

fiber between RN_j and RN_{j+1}. On the other hand, for the downstream signals in the lower branch of the ring network, the operating principle is very similar to that for the downstream signals in the upper branch except for the direction of propagation of the signals.

However, it should be noted that the downstream signals from RN_p cannot be transmitted to RN_{p+1} because OS9 of RN_{p+1} is in working state 2, in which it is cross connected. In cooperation with the working state of OS9, these signals will instead reach port 1 of coupler 1 and then be simultaneously transmitted to the output ports of WS1 and WS2 and port 3 of OS12. Similarly, the downstream signals from RN_{p+1} cannot be transmitted to RN_p because OS9 of RN_p is in working state 1.

A schematic of an ONU is depicted in Fig. 6. The ONU consists of one coarse wavelength division multiplexer (CWDM), one photoelectric detector (PD), one splitter, one RSOA, one antenna, one optical receiver, one tunable transmitter, two circulators and one duplexer. Here, Rx_1 is used to receive the baseband signals coming from the RN, and the tunable Tx_1 is used to remodulate the radio signals received by the antenna to a specified wavelength for forming upstream signals.

Taking ONU_j^i as an example, the downstream signals coming from the AWG of RN_j will be demultiplexed into two signals (λ_{rj}^i and λ_{bj}^i) at different wavelengths by the CWDM. The radio signals output from port 3 of the CWDM first pass through circulator 2 and then undergo photovoltaic conversion and reamplification by the PD. After amplification, the radio signals will pass to the duplexer and then be transmitted by the antenna. Meanwhile, the baseband signals output from port 2 of the CWDM first pass through circulator 1 and then reach port 1 of the splitter. After these signals are output from ports 2 and 3 of the splitter, they will be separated into two parts with equal optical power. One part enters Rx_1, and the other part is injected into the RSOA and is remodulated to become part of the upstream signals.

On the other hand, the baseband signals remodulated by the RSOA will first sequentially pass through the splitter and circulator 1 and then be transmitted to the CWDM to form one part of the upstream signals. Meanwhile, the radio signals received by the antenna will reach the tunable Tx_1 after being output from port 3 of the duplexer and will then be remodulated to also form part of the upstream signals. Note that the emission wavelength of Tx_1 is adjusted to λ_{rj}^i at this point. After these signals (the baseband signals and the radio signals) are multiplexed to form the upstream signals by the CWDM and are output from its port 1, they will pass to the AWG through the distribution fiber between ONU_j^i and RN_j and then pass through circulator 1 in RN_j. At this time, because the upstream signals enter port 2 of circulator 1, they will be output from its port 1 and then pass through coupler 2, OS10 and switch B successively. Finally, the upstream signals from RN_j will propagate to the CO along the inner fiber together with the upstream signals from the other RNs ($RN_{j+1} - RN_p$) in the upper branch of the ring network. Note that the operating principle for the upstream

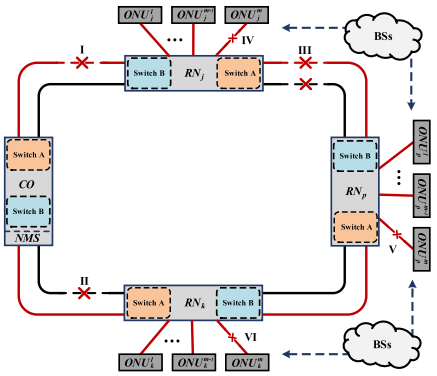

FIGURE 7. Diagram of fault locations.

signals in the lower branch of the ring network is very similar to that for the upstream signals in the upper branch except for the direction of propagation of the signals. Therefore, we will not go into further detail here.

III. PROTECTION MECHANISMS

The possible operating scenarios of the network can be divided into the normal scenario and various fault scenarios. The operating principle of the network in the normal scenario has been introduced in the previous section, whereas the protection mechanisms adopted in fault scenarios will be elaborated in this section. These protection mechanisms can be classified into three types according to the locations of the faults, namely, single-fiber fault protection, dual-fiber fault protection and distribution-fiber fault protection. Corresponding to the specific locations of the faults, the states of the devices in the various network operating scenarios are summarized in Table 2.

Table 2 lists six representative fault locations, which can represent any type of fault in the network, to facilitate the overall illustration of the network operating principles. Note that there are three possible working states for each of the tunable FBGs: in the first, they are adjusted to a specified wavelength to reflect a specified input signal; in the second, they are allowed to be adjusted to any arbitrary wavelength, as expressed by the symbol "\"; and in the third, they are allowed to be adjusted to any wavelength other than the wavelength of the signals output by coupler 3 of the RN, as expressed by the symbol "×". For convenience, we assume here that the network consists of one CO and three RNs (RN_j, RN_p, and RN_k), which are adjacent to each other. In addition, each of the RNs is connected to three ONUs. Accordingly, the network is divided into an upper branch ($CO-RN_j-RN_p$) and a lower branch ($CO-RN_k$). In addition, between each pair of adjacent RNs, BSs are deployed to provide microwave protection against faults occurring in the distribution fibers of the star network, as shown in Fig. 7. In the following subsections, we will discuss the protection mechanisms applied for different fault locations in detail.

A. SINGLE-FIBER FAULT PROTECTION

When a single-fiber fault occurs in the ring network, normal communication in the network can be recovered by applying the following protection mechanism. There are two possible situations: one in which the outer fiber of the ring architecture is broken between adjacent RNs and one in which the fault occurs on the inner fiber between adjacent RNs. Here, we assume that the outer-fiber fault (fault I) is located on the outer fiber between the CO and RN_j and that the inner-fiber fault (fault II) is located on the inner fiber between the CO and RN_k, as shown in Fig. 7.

If fault I occurs, then the modes of switch A of the CO and switch B of RN_j need to be changed under the control of the NMS. According to the protection mechanism, both switch A and switch B should be switched to mode 3. Under these conditions, the downstream signals will propagate from the CO to RN_j via the inner fiber between the CO and RN_j in the clockwise direction, whereas the upstream signals will still propagate via the inner fiber in the counterclockwise direction. In this way, the normal communication of the network will be unaffected by fault I.

If the fault occurs in the location of fault II, then both switch B of the CO and switch A of RN_k should be switched to mode 2. In this case, the downstream signals will still be transmitted from the CO to RN_k through the outer fiber in the counterclockwise direction. However, the upstream signals will be transmitted to the CO through the outer fiber between the CO and RN_k in the clockwise direction. By transferring the upstream signals to the outer fiber, normal communication can be restored.

It should be noted that the network can also be restored even if single faults occur in multiple segments of the dual-ring architecture. For this purpose, it is necessary only to change the working modes of switches A and B of the adjacent RNs. Since the fiber through which the signals propagate is determined only by the working modes of switches A and B of the adjacent RNs, the propagation of the signals in each segment of the dual-ring structure is mutually independent.

B. DUAL-FIBER FAULT PROTECTION

When a dual-fiber fault occurs in the ring network, in which both the outer fiber and the inner fiber between adjacent RNs are broken simultaneously, the upper and lower branches of the dual-ring architecture will be rebuilt to maintain normal communication in the network. For example, suppose that a dual-fiber fault (fault III) occurs in the segment between RN_j and RN_p, as shown in Fig. 7. According to the protection mechanism, OS9 and OS10 in RN_p should be switched to state 2. In this case, the ring network is divided into an upper branch ($CO-RN_j$) and a lower branch ($CO-RN_k-RN_p$). In the upper branch, the downstream signals are transmitted from the CO to RN_j in the clockwise direction along the outer fiber, whereas the upstream signals are transmitted in the counterclockwise direction along the inner fiber. The propagation direction of the signals in the lower branch is opposite

TABLE 2. Device states in various network operating scenarios.

Device		Operating scenarios						
		Normal	Fault I	Fault II	Fault III	Fault IV	Fault V	Fault VI
CO	Switch A	mode 1	mode 3	mode 1	mode 1	mode 1	mode 1	mode 1
	Switch B	mode 1	mode 1	mode 2	mode 1	mode 1	mode 1	mode 1
RN_j	Switch A	mode 1	mode 1	mode 1	mode 1	mode 1	mode 1	mode 1
	Switch B	mode 1	mode 3	mode 1	mode 1	mode 1	mode 1	mode 1
	OS 9	state 1	state 1	state 1	state 1	state 1	state 1	state 1
	OS 10	state 1	state 1	state 1	state 1	state 1	state 1	state 1
	OS 11	state 1	state 1	state 1	state 1	state 1	state 1	state 1
	OS 12	state 1	state 1	state 1	state 1	state 2	state 1	state 1
	FBG 1	×	×	×	×	λ_{rj}^{m}	×	×
	FBG 2	\	\	\	\	\	λ_{rp}^{m}	\
	FBG 3	\	\	\	\	\	\	\
RN_p	Switch A	mode 1	mode 1	mode 1	mode 1	mode 1	mode 1	mode 1
	Switch B	mode 1	mode 1	mode 1	mode 1	mode 1	mode 1	mode 1
	OS 9	state 1	state 1	state 1	state 2	state 1	state 1	state 2
	OS 10	state 1	state 1	state 1	state 2	state 1	state 1	state 2
	OS 11	state 1	state 1	state 1	state 2	state 2	state 1	state 1
	OS 12	state 1	state 1	state 1	state 1	state 1	state 1	state 1
	FBG 1	×	×	×	×	×	λ_{rp}^{m}	λ_{rk}^{m}
	FBG 2	\	\	\	\	\	\	\
	FBG 3	\	\	\	\	λ_{rj}^{m}	\	\
RN_k	Switch A	mode 1	mode 1	mode 2	mode 1	mode 1	mode 1	mode 1
	Switch B	mode 1	mode 1	mode 1	mode 1	mode 1	mode 1	mode 1
	OS 9	state 2	state 2	state 2	state 2	state 2	state 2	state 2
	OS 10	state 2	state 2	state 2	state 2	state 2	state 2	state 2
	OS 11	state 1	state 1	state 1	state 1	state 1	state 1	state 1
	OS 12	state 1	state 1	state 1	state 1	state 1	state 1	state 1
	FBG 1	×	×	×	×	×	×	×
	FBG 2	\	\	\	\	\	\	λ_{rk}^{m}
	FBG 3	\	\	\	\	\	\	\

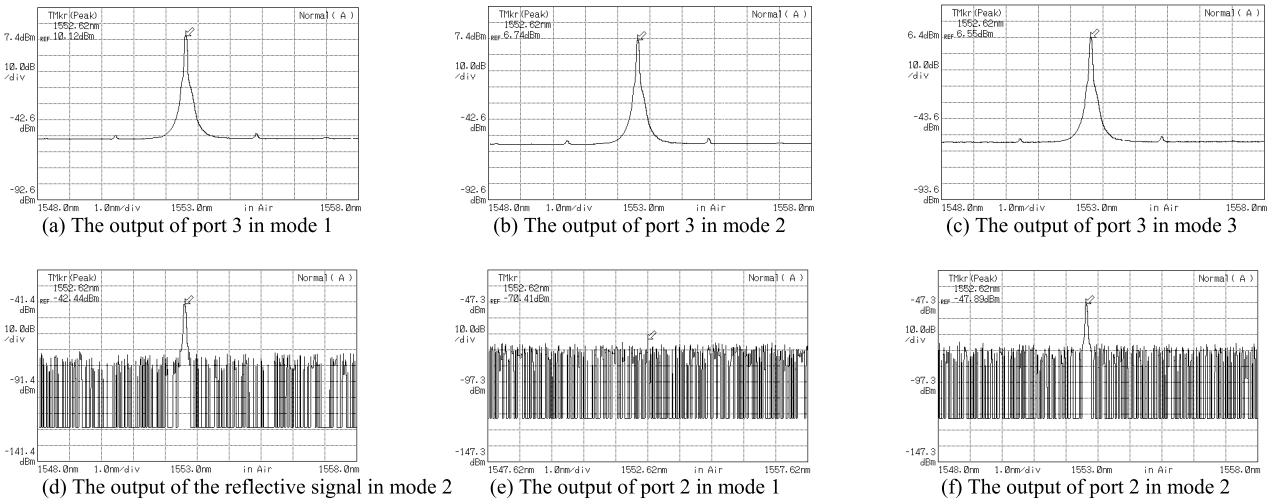

(a) The output of port 3 in mode 1
(b) The output of port 3 in mode 2
(c) The output of port 3 in mode 3
(d) The output of the reflective signal in mode 2
(e) The output of port 2 in mode 1
(f) The output of port 2 in mode 2

FIGURE 8. Experimental results for the OSM.

to that of the signals in the upper branch. By this means, normal communication in the network can be maintained, even for signals that would not need to pass through the dual fiber between RN_j and RN_p in the normal scenario.

In fact, recovery from a dual-fiber fault located anywhere in the ring network can be achieved by changing the operating states of OS9 and OS10 in neighboring RNs. However, in the situation in which multiple dual-fiber faults occur at the same time, the proposed protection mechanism cannot meet the requirements for failure recovery.

C. DISTRIBUTION-FIBER FAULT PROTECTION

When the distribution fiber between an RN and an ONU is broken, the communication between the ONU and the

CO can be recovered by means of microwave protection. According to the location of the RN to which the distribution fiber belongs, there are three possible types of locations of distribution-fiber faults, which correspond to different protection mechanisms. In the proposed network architecture, by default, an ONU in the upper branch of the ring architecture is wirelessly protected by an ONU of the adjacent RN in the counterclockwise direction, whereas an ONU in the lower branch of the ring architecture is wirelessly protected by an ONU of the adjacent RN in the clockwise direction. However, there are two locations that are exceptions to these rules because they cannot receive effective protection in this way. The first is the starting RN along the clockwise direction in the upper branch, and the other is the starting RN along the counterclockwise direction in the lower branch. Here, to fully describe the protection mechanisms for distribution-fiber faults, we consider fault IV, located on the distribution fiber between RN_j and ONU_j^m; fault V, located on the distribution fiber between RN_p and ONU_p^m; and fault VI, located on the distribution fiber between RN_k and ONU_k^m, as shown in Fig. 7.

If fault IV occurs, it can only be wirelessly protected against by ONU_p^m associated with RN_p because ONU_j^m is connected to the starting RN along the clockwise direction in the upper branch. According to the protection mechanism, OS12 of RN_j should be switched to state 2, and the wavelength reflected by FBG1 should be adjusted to λ_{rj}^m. In addition, OS11 of RN_p should be switched to state 2, and the wavelength reflected by FBG3 should be adjusted to λ_{rj}^m. In this way, the radio signals transmitted to ONU_j^m as part of the downstream signals output from coupler 3 will be reflected by FBG1 of RN_j and then pass through OS12 and coupler 1. After coupling with the downstream signals, the signals will sequentially pass through OS9 and switch A and next will reach RN_p along the outer fiber of the ring architecture. In RN_p, since the wavelength reflected by FBG3 has been adjusted to λ_{rj}^m, the reflected signal from RN_j will be reflected again and reach coupler 3. After coupling with the downstream signals, because FBG1 has been adjusted to any wavelength other than the wavelength of the signals output by coupler 3, the reflected signals will pass through circulator 1 and then be demultiplexed by the AWG. Finally, since the wavelength interval between λ_{rj}^m and λ_{rj}^p is one FSR, the reflected radio signal can be injected into ONU_p^m and transmitted to ONU_j^m through the BSs to realize microwave protection. Regarding the upstream signals of ONU_j^m, they will first be transmitted to ONU_p^m by the BSs and received by its antenna. Next, the received signals will pass through the duplexer and be modulated by the tunable optical Tx_1 into optical signals with a wavelength of λ_{rj}^m. Finally, they will return to the CO together with the other upstream signals after passing through circulator 2 and the CWDM. Notably, since the wavelength of the downstream signals transmitted to ONU_p^m is not the same as the wavelength reflected by either FBG3 or FBG2, this protection mechanism does not affect the transmission of normal downstream signals.

If fault V occurs, the communication between ONU_p^m and the CO can be recovered by means of microwave protection from ONU_j^m associated with RN_j. According to the protection mechanism, both the wavelength reflected by FBG2 of RN_j and that reflected by FBG1 of RN_p should be adjusted to λ_{rp}^m. In this case, in RN_p, the transmission path of the radio signals transmitted to ONU_p^m will be $FBG1 \rightarrow OS12 \rightarrow Coupler\ 2 \rightarrow OS10 \rightarrow Switch\ B \rightarrow RN_j$. In RN_j, since the wavelength reflected by FBG2 has been adjusted to λ_{rp}^m, the reflected signal from RN_p will be reflected again and reach coupler 3 together with the downstream signals output from port 3 of WS2. Since FBG1 has been adjusted to the same state as in the case of fault IV, the transmission path of the reflected signals is $FBG1 \rightarrow Circulator\ 1 \rightarrow AWG \rightarrow ONU_j^m \rightarrow BSs \rightarrow ONU_p^m$. This protection mechanism does not affect normal downstream communication due to a principle similar to that in the case of fault IV.

If fault VI occurs, the communication between ONU_k^m and the CO can be recovered by means of microwave protection from ONU_p^m associated with RN_p. Because fault VI is located at the starting RN along the counterclockwise direction in the lower branch and there is no more than one RN in the lower branch of the ring architecture, OS9 and OS10 of RN_p should first be switched to state 2 according to the protection mechanism. In this way, the architecture of the ring network will be divided into a new upper branch ($OLT - RN_j$) and lower branch ($OLT - RN_k - RN_p$). Second, both the wavelength reflected by FBG1 of RN_p and that reflected by FBG2 of RN_k should be adjusted to λ_{rk}^m. In this case, in RN_k, the transmission path of the radio signals transmitted to ONU_k^m will be $FBG1 \rightarrow OS12 \rightarrow Coupler\ 1 \rightarrow OS9 \rightarrow Switch\ A \rightarrow RN_p$. In RN_p, since the wavelength reflected by FBG3 has been adjusted to λ_{rk}^m, the reflected signal from RN_k will be reflected again and reach coupler 3 together with the downstream signals output from port 3 of WS2. Since FBG1 has been adjusted to the same state as in the case of fault IV, the transmission path of the reflected signals is $FBG1 \rightarrow Circulator\ 1 \rightarrow AWG \rightarrow ONU_p^m \rightarrow BSs \rightarrow ONU_k^m$. Since the wavelength of the upstream signals from ONU_k^m is not the same as the wavelength reflected by either FBG1 or FBG2, this protection mechanism does not affect upstream communication.

It should be noted that because the propagation direction of the radio signals reflected by an FBG always remains the same as that of the upstream signals or downstream signals, the influence of RB can be completely mitigated in these protection mechanisms for distribution fibers. In addition, these protection mechanisms can be easily extended to networks of larger scales because the discussion of the above three types of faults covers all possible situations.

IV. BANDWIDTH ALLOCATION SCHEME

In our paper, the network architecture adopts the scheme of bandwidth allocation with the wavelength as the minimum scheduling unit. The bandwidth allocation in various operating scenarios is listed in Table 3. It can be seen that

TABLE 3. Bandwidth allocation in various network operating scenarios.

Device		Operating scenarios							
		Fault IV		Fault V		Fault VI		Other scenarios	
RN_j	ONU_j^1	$\lambda_{rj}^{\ 1}$	$\lambda_{bj}^{\ 1}$	$\lambda_{rj}^{\ 1}$	$\lambda_{bj}^{\ 1}$	$\lambda_{rj}^{\ 1}$	$\lambda_{bj}^{\ 1}$	$\lambda_{rj}^{\ 1}$	$\lambda_{bj}^{\ 1}$
	ONU_j^{m-1}	$\lambda_{rj}^{\ m-1}$	$\lambda_{bj}^{\ m-1}$	$\lambda_{rj}^{\ m-1}$	$\lambda_{bj}^{\ m-1}$	$\lambda_{rj}^{\ m-1}$	$\lambda_{bj}^{\ m-1}$	$\lambda_{rj}^{\ m-1}$	$\lambda_{bj}^{\ m-1}$
	ONU_j^m	×	×	$\lambda_{rp}^{\ m}$	$\lambda_{bj}^{\ m}$	$\lambda_{rj}^{\ m}$	$\lambda_{bj}^{\ m}$	$\lambda_{rj}^{\ m}$	$\lambda_{bj}^{\ m}$
RN_p	ONU_p^1	$\lambda_{rp}^{\ 1}$	$\lambda_{bp}^{\ 1}$	$\lambda_{rp}^{\ 1}$	$\lambda_{bp}^{\ 1}$	$\lambda_{rp}^{\ 1}$	$\lambda_{bp}^{\ 1}$	$\lambda_{rp}^{\ 1}$	$\lambda_{bp}^{\ 1}$
	ONU_p^{m-1}	$\lambda_{rp}^{\ m-1}$	$\lambda_{bp}^{\ m-1}$	$\lambda_{rp}^{\ m-1}$	$\lambda_{bp}^{\ m-1}$	$\lambda_{rp}^{\ m-1}$	$\lambda_{bp}^{\ m-1}$	$\lambda_{rp}^{\ m-1}$	$\lambda_{bp}^{\ m-1}$
	ONU_p^m	$\lambda_{rj}^{\ m}$	$\lambda_{bp}^{\ m}$	×	×	$\lambda_{rk}^{\ m}$	$\lambda_{bp}^{\ m}$	$\lambda_{rp}^{\ m}$	$\lambda_{bp}^{\ m}$
RN_k	ONU_k^1	$\lambda_{rk}^{\ 1}$	$\lambda_{bk}^{\ 1}$	$\lambda_{rk}^{\ 1}$	$\lambda_{bk}^{\ 1}$	$\lambda_{rk}^{\ 1}$	$\lambda_{bk}^{\ 1}$	$\lambda_{rk}^{\ 1}$	$\lambda_{bk}^{\ 1}$
	ONU_k^{m-1}	$\lambda_{rk}^{\ m-1}$	$\lambda_{bk}^{\ m-1}$	$\lambda_{rk}^{\ m-1}$	$\lambda_{bk}^{\ m-1}$	$\lambda_{rk}^{\ m-1}$	$\lambda_{bk}^{\ m-1}$	$\lambda_{rk}^{\ m-1}$	$\lambda_{bk}^{\ m-1}$
	ONU_k^m	$\lambda_{rk}^{\ m}$	$\lambda_{bk}^{\ m}$	$\lambda_{rk}^{\ m}$	$\lambda_{bk}^{\ m}$	×	×	$\lambda_{rk}^{\ m}$	$\lambda_{bk}^{\ m}$

the bandwidth allocation follows the scheme of wavelength assignment described in section II when the network operates in the normal scenario (normal), single-fiber fault scenario (fault I and fault II) and dual-fiber fault scenario (fault III). However, when the network operates in the distribution-fiber fault scenarios (fault IV, fault V and fault VI), the scheme of bandwidth assignment will be adjusted according to the location where the fault occurs and the size of the available bandwidth of the ONUs located in adjacent RNs. In this process, when the NMS ascertains that a fault has occurred, the NMS will first locate the fault, determine which ONU is affected by the fault, and then search for the ONU with the maximum available bandwidth among its ONUs that are located in adjacent RNs (its next-order RN and its front-order RN). Once this optimal ONU is determined, also called the protective ONU, the NMS will reconfigure the entire network to recover the original wireless service belonging to the ONU affected by the fault according to the protection mechanisms described in section III. Taking fault V as an example, here we assume that the ONU_j^m is determined as the protective ONU. The NMS will select λ_{rp}^m to replace the λ_{rj}^m of ONU_j^m in order to provide the original wireless services for users of ONU_p^m, which is achieved by configurating the device states according to Table 2. It should be noted that the protective ONU is preferentially selected from the same branch of the architecture to avoid the deterioration of QoS metrics due to the extra switching time. Thus, ONU_p^m will be determined as the protective ONU if fault IV or fault VI occurs.

V. NETWORK ANALYSIS AND RESULTS

In this section, we will discuss the network performance in terms of OSM performance, power loss, network reliability and optical transmission performance.

A. OSM PERFORMANCE

The OSM is an important device for realizing fault protection in the network architecture proposed in this paper, and its performance can greatly affect the performance of the entire network. In this section, we report experimental tests of the performance indicators of the OSM, including the insertion loss (IL), return loss (RL), isolation, crosstalk, and switching time. The experimental equipment used in this experiment included an Anritsu MS9710C optical spectrum analyzer, a Thorlabs TLX1 tunable laser source, mechanical OSs, a 5 V DC power supply and optical fiber connectors. The optical spectrum analyzer works in the C waveband range of 600 $\sim$ 1750 nm, and it can detect optical power between -90 dBm and 20 dBm. The tunable laser source works in the C waveband range of 1528 $\sim$ 1566 nm and possesses a linewidth of 10 kHz. The power supply was used to provide a 5 V DC voltage to control the working mode of the OSM. In the course of the experiment, the optical path connections of the OSM were as shown in Fig. 4 in section II, and it could be switched among each of its working modes by using voltage levels of 5 V or GND. The working wavelength of the laser was set to 1552.62 nm, and its transmit power was 11.99 dBm. Here, we tested the performance of the OSM in each of its working modes by performing the following three experimental steps. First, we input the signals generated by the laser into port 1 of the OSM. Second, the optical spectrum analyzer was used to collect data from each of the ports of the OSM in the different working modes. Third, the reflected signals used to calculate the RL were collected by a circulator connected to port 1 of the OSM. For simplicity, not all experimental results are shown. Selected results for the OSM are shown in Fig. 8.

In Fig. 8, Fig. 8 (a) $\sim$ (c) show the results for the downstream signals output in each of the working modes, which can be used to determine the IL. Fig. 8 (d) shows the measurement results for the reflected signal passing through the circulator. Fig. 8 (e) and Fig. 8 (f) show the results for the outputs of port 3 in mode 1 and of port 2 in mode 2, respectively. Based on the complete experimental results for the OSM and the transmit power of the laser, the performance indicators in each of the working modes could be calculated, as listed in detail in Table 4.

As seen in Table 4, the value of the IL (L_{OSM}^1) is 1.87 dB in the normal mode (mode 1), which is the lowest value among all modes. Similarly, the other performance indicators observed in mode 1 are also superior to those in the other

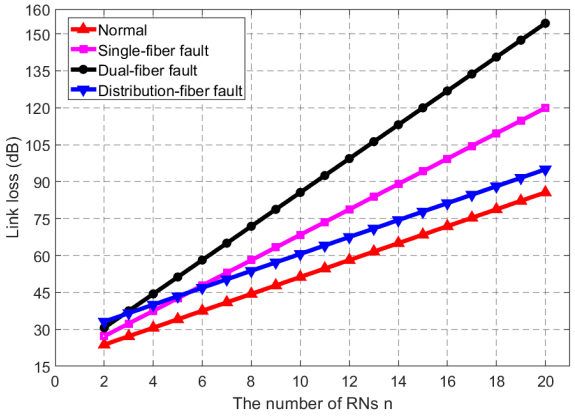

FIGURE 9. Losses in the four operating scenarios.

TABLE 4. Performance indicators of the OSM.

Performance indicator	Working mode of the OSM		
	Mode 1	Mode 2	Mode 3
Insertion loss	1.87 dB	5.25 dB	5.30 dB
Return loss	51.20 dB	54.43 dB	50.55 dB
Isolation	80.53 dB	54.63 dB	55.07 dB
Crosstalk	-82.40 dB	-59.88 dB	-60.51 dB
Switching time	\	48 ms	32 ms

two modes. This is because in mode 1, the signals must pass through the fewest OSs compared with the other modes. However, although all performance indicators in modes 2 and 3 are worse than those in mode 1, they can still satisfy the needs of normal communication. For instance, the maximum time required to switch the operating mode is 48 ms, which is less than the time limit of 50 ms for maintaining normal communication. In addition, the ILs in modes 2 and 3 (L^2_{OSM} and L^3_{OSM}) can be compensated by deploying a suitable number of EDFAs and adjusting the amplification gain. Note that if OSs based on microelectromechanical systems (MEMS) were to be adopted instead of mechanical OSs, the switching time of the OSM could be further reduced to meet the needs of high-speed communication. Consequently, the designed OSM can effectively satisfy the requirements for fault protection in the ring network.

B. NETWORK SCALE ANALYSIS

Link loss is a significant factor limiting network scale, including the distance of transmission and the number of RNs supported. Therefore, in this section, we first calculate the maximal power budget in different network operating scenarios and then determine the number and gain of the EDFAs by analyzing the network scale based on the proposed network architecture. In accordance with the network operating principles as illustrated in sections II and III, the possible operating scenarios can be divided into four types to discuss the corresponding link losses, namely, the normal scenario, single-fiber fault protection, dual-fiber fault protection and distribution-fiber fault protection. Here, we use d_1 to denote the distance between the CO and an adjacent RN or between

TABLE 5. IL values of optical components.

Component	Symbol	Insertion loss	References
AWG	L_{AWG}	3 dB	[40]
Splitter	$L_{Splitter}$	3 dB	[40]
CWDM	L_{CWDM}	0.5 dB	[40]
Circulator	$L_{Circulator}$	0.5 dB	[40]
Coupler	$L_{Coupler}$	0.5 dB	[40]
WS	L_{WS}	2 dB	[12]
OS	L_{OS}	0.5 dB	[15]
FBG	L_{FBG}	3.5 dB	[41]
Fiber (km)	α	0.2 dB	[15]

adjacent RNs. The length of the distribution fiber between an RN and an ONU is denoted by d_2. Specifically, we assume that $d_1 = 5$ km, $d_2 = 2$ km, and $p = n/2$. The IL of each component used in the network is listed in Table 5.

When the network is operating in the normal scenario, the signals propagating between the CO and an ONU connected to RN_p will suffer the maximum power loss L^1_{Tmax}, which can be calculated as follows:

$$\begin{aligned} L^1_{T\max} &= (3p-1)L_{OS} + p(L^1_{OSM} + L_{Coupler} + L_{WS}) + 2\times L_{Circulator} \\ &\quad + 2\times L_{AWG} + 2\times L_{Splitter} + L_{FBG} + L_{CWDM} + \alpha\times(pd_1 + d_2). \end{aligned} \tag{1}$$

When the network is operating in the single-fiber fault protection scenario, the worst possible case is that a single-fiber fault has occurred in each segment connecting adjacent RNs. Because the ILs of the OSM when working in mode 2 and mode 3 are approximately equal, the same analysis method can be used to evaluate the power loss for both an outer-fiber fault and an inner-fiber fault. Therefore, an ONU connected to RN_p has the maximum power loss L^2_{Tmax}, which can be calculated as follows:

$$\begin{aligned} L^2_{T\max} &= (3p-1)L_{OS} + p(L^2_{OSM} + L_{Coupler} + L_{WS}) + 2\times L_{Circulator} \\ &\quad + 2\times L_{AWG} + 2\times L_{Splitter} + L_{FBG} + L_{CWDM} + \alpha\times(pd_1 + d_2). \end{aligned} \tag{2}$$

When the network is operating in the dual-fiber fault protection scenario, the worst possible case is that a dual-fiber fault has occurred in a segment connecting the CO to an RN. In this case, the signals must pass through the entire ring architecture before reaching the target ONU. Therefore, an ONU connected to RN_1 or RN_n has the maximum power loss L^3_{Tmax}, which can be calculated as follows:

$$\begin{aligned} L^3_{T\max} &= (3n-1)L_{OS} + n(L^1_{OSM} + L_{Coupler} + L_{WS}) + 2\times L_{Circulator} \\ &\quad + 2\times L_{AWG} + 2\times L_{Splitter} + L_{FBG} + L_{CWDM} + \alpha\times(nd_1 + d_2). \end{aligned} \tag{3}$$

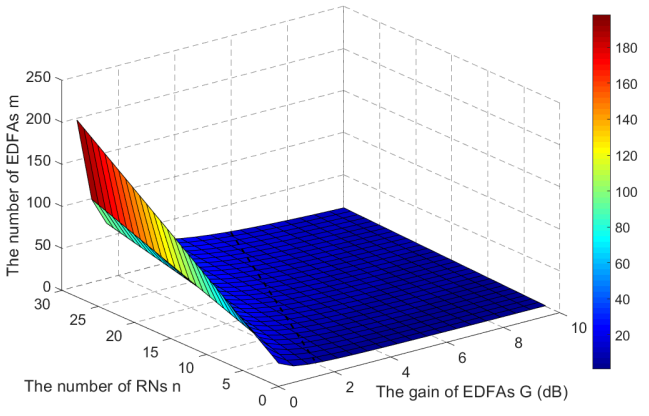

FIGURE 10. Relationship among *G*, *n* and *m*.

When the network is operating in the distribution-fiber fault protection scenario, the situation is similar to the normal scenario. Thus, an ONU connected to RN_p will suffer the maximum power loss L^4_{Tmax}, which can be calculated as follows:

$$\begin{aligned} L^4_{T\max} &= (3p+2)L_{OS}+(p+1)L^1_{OSM}+(p+2)L_{Coupler}+3\times L_{FBG} \\ &\quad +2\times L_{AWG}+pL_{WS}+2\times L_{Circulator}+L_{Splitter}+L_{CWDM} \\ &\quad +\alpha\times[(p+1)d_1+d_2]. \end{aligned} \tag{4}$$

According to the above analysis, among all four operating scenarios, the power loss in the dual-fiber fault protection scenario is the largest. Furthermore, we can obtain the detailed relation between the number of RNs and the maximum power loss for each of the four scenarios, as shown in Fig. 9. Note that the number of RNs in the proposed network architecture can be no fewer than two.

The power budget for the downstream signals must satisfy the following inequality:

$$P_T - L_M - L_T + mG \geq P_r. \tag{5}$$

Here, P_T, L_M, P_r, and G denote the transmit power of the transmitter, the power redundancy of the system, the receiver sensitivity and the gain of the EDFAs, respectively. m represents the total number of EDFAs adopted in the network. Specifically, we assume that $P_T = 0$ dBm, $L_M = 5$ dB, and $P_r = -30$ dBm. Moreover, for convenience, we assume that each RN has one EDFA to amplify the downstream signals. In this case, $m = n$. Thus, we can obtain

$$G \geq (-25 + L_T)/n. \tag{6}$$

By substituting (4) into (5), the relationship among G, n and m can be determined, as shown in Fig. 10. From this figure, we can see that once the gain of the EDFAs reaches a certain value, the total number of EDFAs employed in the network will remain constant as the number of RNs increases. The values of the gain of the EDFAs corresponding to different numbers of RNs are represented by the black dotted line in Fig. 10. Although the gain of the EDFAs slowly increases with an increasing number of RNs, the EDFA gain that is typically adopted in actual applications is much higher than that value. Therefore, the number of EDFAs can be approximately considered to remain unchanged with a varying number of RNs. This demonstrates that not every RN in the network to have an EDFA. Hence, not only can the construction cost of the network be reduced, but the limit on the number of EDFA cascades can also be alleviated in the large scale network, thus further improving the scale of the network. Note that the numerical values in Fig. 10 are valid only for the case of $n \geq m$ because each RN is considered to have at most one EDFA to compensate for the loss of the downstream signals in the network.

TABLE 6. Unavailability data for optical components.

Component	Symbol	Unavailability (Failure/10^9h)	References
OLT	U_{OLT}	5.12×10^{-7}	[40]
EDFA	U_{EDFA}	4×10^{-7}	[40]
Circulator	U_{Cir}	2×10^{-7}	[40]
Coupler	U_{Cpl}	4×10^{-8}	[40]
Splitter	U_{Spl}	4×10^{-8}	[40]
WS	U_{WS}	4×10^{-7}	[12]
OS	U_{OS}	4×10^{-7}	[15]
FBG	U_{FBG}	1×10^{-7}	[41]
ONU	U_{ONU}	5.12×10^{-7}	[15]
AWG	U_{AWG}	4.8×10^{-6}	[40]
Wireless link	U_{Wir}	3.3×10^{-5}	[30]
CWDM	U_{CWDM}	1.44×10^{-5}	[13]
Fiber (km)	U_F	2.4×10^{-7}	[15]

C. NETWORK RELIABILITY ANALYSIS

The network reliability is limited by many internal factors, including the service times and manufacturing processes of the optical components themselves, which are key factors that should be taken into consideration when designing the network architecture. Thus, in the following, the network reliability will be discussed in detail. The unavailability data and the symbols used to represent the optical components employed in the network architecture are listed in Table 6.

Here, U_{CO} denotes the unreliability of the CO, and U_{CO-RN_j} and U'_{CO-RN_j} denote the unreliability of the components from the CO to RN_j in the clockwise direction and the counterclockwise direction, respectively. Similarly, $U_{RN_j-RN_{j+1}}$ and $U'_{RN_j-RN_{j-1}}$ denote the unreliability of the segments from RN_j to RN_{j+1} in the clockwise direction and from RN_j to RN_{j-1} in the counterclockwise direction, respectively. U_{RN_j-ONU}, $U_{RN_{j+1}-ONU}$ and $U'_{RN_{j-1}-ONU}$ denote the unreliability of the segments from RN_j to an ONU, from RN_{j+1} to an ONU and from RN_{j-1} to an ONU, respectively.

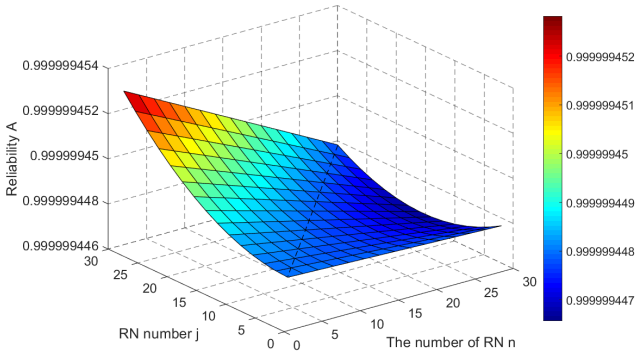

FIGURE 11. Relationship among *A*, *j*, and *n*.

Thus, taking an ONU connected to RN_j $(2 \le j \le n)$ as an example, the unreliability U of the network is

$$U = U_{CO} + U_{CO-RN_j} \times U'_{CO-RN_j} + U_{RN_j-ONU} \times (U'_{RN_j-RN_{j-1}} + U'_{RN_{j-1}-ONU}) \times (U_{RN_j-RN_{j+1}} + U_{RN_{j+1}-ONU}), \quad (7)$$

where

$$U_{CO} = U_{OLT} + U_{Spl}, \quad (8)$$

$$U_{CO-RN_j} = [4 \times U_{OS} + (2 \times U_{Cir} + d_1 \times U_F)(4 \times U_{OS} + 2 \times U_{Cir} + d_1 \times U_F) + U_{EDFA} + U_{WS} + U_{Cpl}] \times j + U_{FBG}, \quad (9)$$

$$U'_{CO-RN_j} = [4 \times U_{OS} + (2 \times U_{Cir} + d_1 \times U_F)(4 \times U_{OS} + 2 \times U_{Cir} + d_1 \times U_F) + U_{EDFA} + U_{WS} + U_{Cpl}] \times (n - j + 1) + U_{FBG}, \quad (10)$$

$$U_{RN_j-ONU} = U_{AWG} + d_2 \times U_F + U_{CWDM} + 3 \times U_{Cir} + U_{Spl} + 2 \times U_{ONU}, \quad (11)$$

$$U'_{RN_j-RN_{j-1}} = 5 \times U_{OS} + (2 \times U_{Cir} + d_1 \times U_F) \times (4 \times U_{OS} + 2 \times U_{Cir} + d_1 \times U_F) + 2 \times U_{Cpl} + 2 \times U_{FBG} + U_{EDFA}, \quad (12)$$

$$U_{RN_j-RN_{j+1}} = 5 \times U_{OS} + (2 \times U_{Cir} + d_1 \times U_F) \times (4 \times U_{OS} + 2 \times U_{Cir} + d_1 \times U_F) + 2 \times U_{Cpl} + 2 \times U_{FBG} + U_{EDFA} + U_{WS}, \quad (13)$$

$$U'_{RN_{j-1}-ONU} = U_{RN_{j+1}-ONU} = U_{RN_j-ONU} + U_{Wir}, \quad (14)$$

Therefore, the network reliability A is

$$A = 1 - U. \quad (15)$$

The relationship among A, n and j can be determined from (15) and is plotted in Fig. 11. From Fig. 11, we can see that the ONUs connected to any RN in the proposed network can meet the five-nines requirement of telecom operators for network reliability. In addition, the reduction in network reliability with a growing number of RNs is very slow. Consequently, even if the number of RNs further increases, the proposed network can still maintain a high degree of reliability. It should be noted that the numerical values in Fig. 11 are valid only in the case of $n \ge j$ because the value of the RN subscript cannot exceed the total number of RNs in the network.

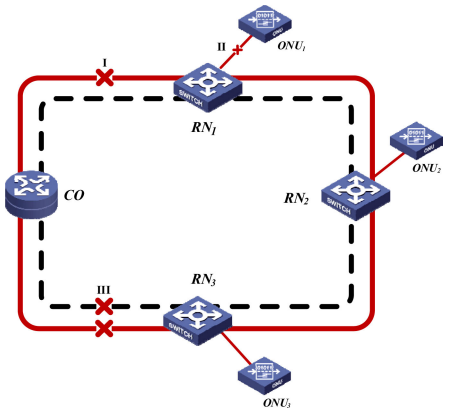

FIGURE 12. Simulation setup representing the proposed architecture.

D. OPTICAL TRANSMISSION PERFORMANCE

The transmission performance of the network was simulated using OptiPerformer. Fig. 12 shows the simulation setup. All fault cases (namely, a single-fiber fault, a dual-fiber fault, and a distribution-fiber fault) are shown. There are three RNs in the ring. Each RN is connected to one ONU. RN_1 and RN_2 belong to the upper branch of the ring, whereas RN_3 is located on the lower branch. Three different operating wavelengths ranging from 1552 to 1553.6 nm with a 0.8 nm spacing are allocated to the three ONUs for generating wired signals. Similarly, another three operating wavelengths ranging from 1568 to 1570.4 nm are allocated for wireless signal access. The wired signals are generated by employing directly modulated lasers operating at 10 Gb/s with $2^9 - 1$ pseudorandom binary sequences (PRBSs) and non-return-to-zero (NRZ) data. The wireless signals are generated by using a dual-arm Mach-Zehnder modulator (D-MZM) driven by two complementary 10 GHz clock signals. OCS is realized by remodulating the signals generated by the directly modulated lasers. The 10 GHz clock signals are generated by a quadrupler and a 2.5 GHz clock. The data rate of the wireless signals is 2.5 Gb/s. The gain of the EDFAs at all RNs is 11 dB. The distance between adjacent RNs (or between the CO and an adjacent RN) is 5 km. The distance between an ONU and its corresponding RN is 2 km. In each ONU, the upstream wavelength is modulated at 2.5 Gb/s with NRZ data.

In Fig. 12, since faults occurring on either the inner or outer fiber can be regarded as the same type of fault scenario when analyzing the transmission performance of the network, the single-fiber fault case can be represented by fault I. Similarly, the dual-fiber and distribution-fiber fault cases can be represented by faults III and II, respectively. In the simulation setup, the generation of upstream optical signals is based on the gain saturation characteristic of the RSOA in order to reuse the wavelength of the downstream optical signals. In this process, the determination of the bias current of the RSOA is critical; it aims to maintain an adequate link gain for upstream transmission and to suppress the downstream data included in the upstream signals. In addition, due to the presence of RB noise, there is an optimal

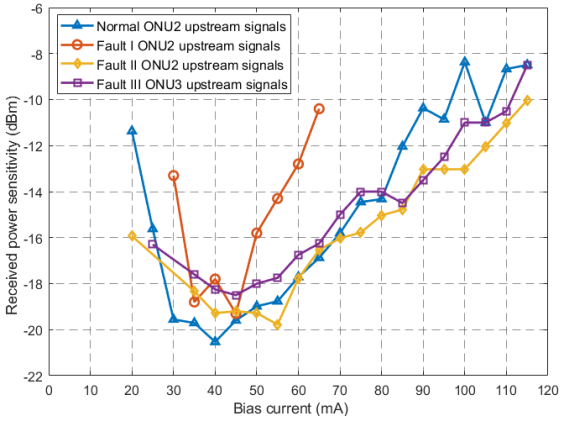

FIGURE 13. Relationship between the bias current and received power sensitivity.

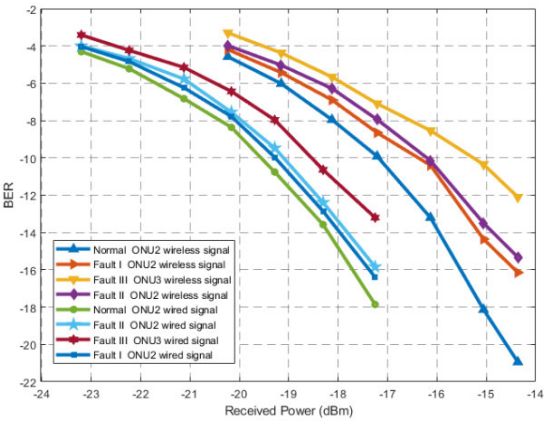

FIGURE 14. BER curves for downstream signals in various operating scenarios.

gain of the RSOA that can make the crosstalk-to-signal ratio of the upstream signals reach the maximum value [18], [19]. Hence, to improve the optical transmission performance with the above comprehensive considerations, the configuration of the related parameters will be discussed in detail. In the simulation setup, the operating temperature is set at 300 K. The pertinent geometrical and material parameters for the RSOA are from [42]. The extinction ratio of the downstream signals is set at 5 dB. The transmit power of the transmitters in the CO is set at 0 dBm. Since the gain of the RSOA can be controlled by the bias current, we select only the bias current as a variable, and we analyze the relationship between the bias current and the received power sensitivity (for BER=10^{-9}) to obtain the appropriate value of the bias current. The worst-case received power sensitivity curves under various operating scenarios are compared, as shown in Fig. 13.

It can be seen from Fig. 13 that there are optimal bias currents in various operating scenarios, which make the received power sensitivity maximal. When the network operates in the normal, fault I, fault II and fault III states, the corresponding optimal bias current values are approximately 40 mA, 45 mA, 55 mA and 45 mA, respectively. Finally, the bias current of 45 mA is selected as the optimal bias current value of the RSOA to simultaneously meet the requirements of multiple operating scenarios. Additionally, the modulated current is set at 20 mA, which determines the extinction ratio of the upstream optical signals.

For convenience, we consider only the ONU with the worst bit error rate (BER) performance in each operating scenario. The worst-case BER curves in the various operating scenarios are shown in Fig. 14.

From Fig. 14, we can see that the BER performance is the best when the network is operating under normal conditions. The BER performance shows a slight decrease when the network is operating in the fault I or fault II scenario. This is because when fault I occurs, the downstream signals sent to ONU_2 will be transmitted through the inner fiber between the CO and RN_1 due to the failure of the outer fiber. In this case, the influence of RB is difficult to mitigate because the downstream signals are transmitted in the clockwise direction in the inner fiber together with the upstream signals being transmitted in the counterclockwise direction in the same fiber. Meanwhile, when fault II occurs, the wireless signals sent to ONU_1 will change their transmission path and propagate to ONU_2. In this case, the wireless signals will propagate together with other downstream signals through a larger number of optical components, such as FBGs, couplers and OSs. This will introduce more link loss, crosstalk and noise into the signals. However, the BER performance in the fault III scenario is the worst. In this case, the overall network cannot be divided into two branches. The signals received by ONU_3 propagate in the clockwise direction through the entire network. Under these conditions, compared with the other operating scenarios, the downstream signals will suffer more serious effects in terms of link loss, noise and accumulation of chromatic dispersion. In addition, Fig. 14 shows that the trend of the BER curves for the wireless signals is the same as that for the wired signals. Moreover, the power penalty between the wired and wireless signals at the given BER of 10^{-9} is approximately 3 dB in each operating scenario. This result is caused by the chromatic dispersion of the two subcarriers, which have a 20 GHz spacing.

The worst-case BER curves for upstream signals are shown in Fig. 15. From this figure, we can see that the performance for upstream signals in the various operating scenarios is always worse than that for downstream signals. This is because the upstream signals are generated via remodulation by the RSOA. In this process, additional power loss and noise can be introduced. Nevertheless, the overall results show that an acceptable performance (BER $< 10^{-9}$) is achieved for all downstream and upstream signals.

E. THE EVALUATION OF THE QUALITY OF SERVICE METRICS

To evaluate the QoS metrics for this protection mechanism, the analysis of the delivery time of packets is very significant. In our mechanisms, the scheme of failure location refers to the method proposed in [43]. Therefore, the total delivery

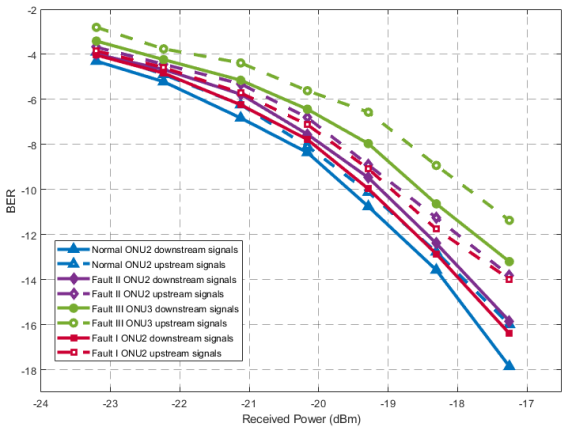

FIGURE 15. BER curves for upstream signals in various operating scenarios.

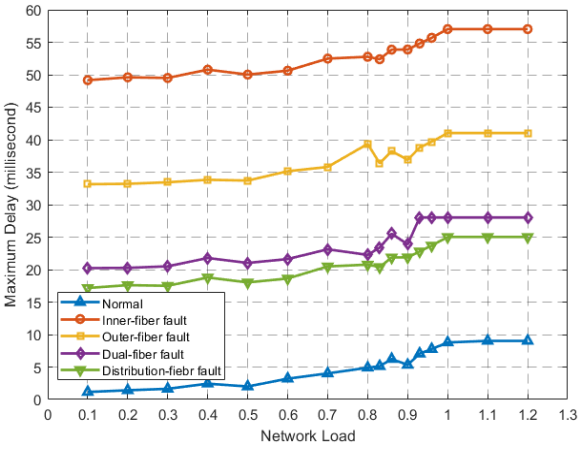

FIGURE 16. Maximum delay for the network in various operating scenarios.

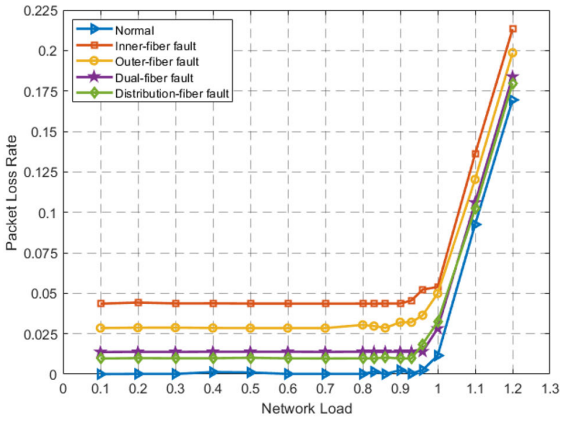

FIGURE 17. Packet loss rate for the network in various operating scenarios.

time consists of four main parts, which are the recovery time T^u_{RTime}, propagation delay T_{PDelay}, packet transmission time T_{PTTime} and queuing delay T_{QDelay}. The superscript u with a value ranging from 1 to 5 represents the normal, inner-fiber fault, outer-fiber fault, dual-fiber fault and distribution-fiber fault operating scenarios, respectively. Although ONUs located in different RNs have different delivery times due to the ring-based architecture, the upper bound of the delivery time in the same operating scenario is the same. Hence, the maximum delay can be calculated as follows:

$$T^u_{MaxDelay} = T^u_{RTime} + T_{PDelay} + T_{PTTime} + T_{QDelay} \quad (16)$$

$$T^1_{RTime} \le RTT + T_c + T_{NMS} + T_{Notify} + T^1_{OSM} \quad (17)$$

$$T^2_{RTime} \le RTT + T_c + T_{NMS} + T_{Notify} + T^2_{OSM} \quad (18)$$

$$T^3_{RTime} \le RTT + T_c + T_{NMS} + T_{Notify} + T^3_{OSM} \quad (19)$$

$$T^4_{RTime} \le RTT + T_c + T_{NMS} + 3 \times T_{Notify} + 2 \times T_{OS} + T_{OTDR1} + T_{OTDR2} \quad (20)$$

$$T^5_{RTime} \le RTT + T_c + T_{NMS} + T_{Notify} + 2 \times T_{OS} \quad (21)$$

where the round-trip time RTT is the longer of the time for a monitoring pulse to travel from the CO to the farthest ONU and the time to cross the ring. T_c is the code duration of the optical code domain reflectometers (OCDRs) in the network, which can prevent the overlapping of the reflected codes [44]. T_{PTTime} is the packet transmission time, and its value depends on the packet size and transmission rate. T_{PDelay} is the propagation time, which depends on the speed in the medium and the distance between the CO and ONU. T_{QDelay} is the time that a packet waits in the queue. T^u_{OSM} is the switching time of the OSM operating in the model u. Similarly, T_{OS} is the switching time of a mechanical optical switch. T_{OTDR1} is the time for monitoring the inner ring by using the optical time domain reflectometer (OTDR). T_{OTDR2} is the time for monitoring the outer ring by using the OTDR. T_{NMS} is the time for the NMS to process the reflected coding signal and locate the fault. T_{Notify} is the time for the NMS to notify devices in the network to change their states.

The QoS metrics of upstream service were evaluated in terms of the maximum delay and packet loss rate under various operating scenarios. The simulation model was developed by using MATLAB and a PC with an i7-8750H CPU and 32 GB RAM. In the simulation setup, the architecture configuration followed the simulation setup described in the previous section V.D. Moreover, the traffic source was modeled by ON/OFF sources with a Pareto distribution to generate self-similar traffic with a Hurst parameter of 0.7 [45]. The packet size was uniformly distributed between 64 and 1518 bytes. In addition, the other system parameters used in the simulation were as follows: (i) The capacity of the upstream service of each ONU contained two wavelengths providing wired service and wireless service, which operated at 2.5 Gb/s; (ii) the queue buffer of the ONU was 5 Mbytes; (iii) the guard time was $T_g = 1\mu$s; (iv) the cycle time was $T_{cycle} = 2$ms; and (v) the simulation time was 1 s. The results of the maximum delay and packet loss rate for the network in various operating scenarios are shown in Fig. 16 and Fig. 17, respectively. The network load is a normalized value, which is the ratio of the traffic generated by the ONUs to the capacity for upstream service.

It can be seen from Fig. 16 that when the network load is light, the maximum delay in the same operating scenario will slowly increase as the network load increases. When the network load is heavy, the maximum delay will rapidly reach a maximum value and remain constant if the network load increases continuously. This is because when the network load is at a relatively low level, the queue buffer is never full within the simulation time. The value of T_{QDelay} is small and maintains a slowly growing tendency. However, if the network load continuously increases until it reaches the status of a full load, due to the full queue buffer, T_{QDelay} will reach the upper-bound value and remain constant. Additionally, at this moment, if the available bandwidth cannot quickly forward the arriving packets, the packet loss will sharply increase, which can also be used to explain the results in Fig. 17. When the network load is light, the packet loss rate remains low and almost unchanged, while the packet loss rate will dramatically increase when the network load approaches full. This turning point in the variation trend of the maximum delay and packet loss rate is almost concurrent.

On the other hand, from Fig. 16 and Fig. 17, there are differences in the QoS metrics between various operating scenarios, which depend on T^u_{RTime}. If the network operates in a normal scenario, T^1_{RTime} will be mainly spent on maintaining the daily detection of faults, and its value will be small. Hence, the maximum delay of operating in a normal scenario is minimal (approximately 9 ms), in contrast to the other scenarios. However, for the fault scenarios, extra time will be taken to perform line switching. In particular, for the inner-fiber fault scenario, since the time-consuming T^2_{OSM} is introduced to T^2_{RTime}, its maximum delay is the largest (approximately 57 ms) compared with the other operating scenarios. Of course, the analysis of the difference in the packet loss rate in various operating scenarios is similar to that of the maximum delay because the longer the recovery time is, the larger the packet loss rate. It should be noted that although our scheme could lead to a potential high recovery time, the switching time of the OSM takes up the majority of the recovery time according to the analysis of the delivery time. In this simulation, the switching time of the OSM was measured by employing many commercial mechanical OSs (the switching time of each OS is not over 8 ms). If OSs with a low switching time are adopted, the recovery time can be further reduced. For instance, if mechanical OSs based on MEMS (where the switching time is 1 ms) [46] are adopted, the maximum delay and packet loss rate of operating in the worst-case situation (where the network load is 1 when the inner-fiber fault occurs) are 15.025 ms and 1.41%, respectively. This means that network operators can make a good tradeoff between the QoS metrics and cost to cater to different requirements from subscribers.

VI. DISCUSSION AND CONCLUSION

The specific objective of this study is to propose an effective protection mechanism for metro-access optical networks based on the WDM technique that satisfies the high reliability requirement of next-generation optical networks. Compared to previous studies, our scheme possesses prominent advantages and differences.

The design of the network architecture needs to consider the tradeoff between additional construction costs and reliability requirements. These are usually contradictory because the improvement of reliability depends on backing up or sharing the existing resources and thus increasing the additional construction cost. In contrast to previous studies based on pure optical protection [9]–[13], [15], [16], [33], [34], [40], [48] and based on wireless protection [21]–[25], [29], [30], our study can enhance the reliability performance for metro-access optical networks based on the WDM technique while reducing the additional construction cost and the expenditure of each subscriber. For example, previous studies [21]–[23] based on survivable WOBAN architecture have the limitation that they are not suitable for fault scenarios that require recovering significant losses of data, such as a fault in the feeder segment and even a fault in the distribution section of the WDM network. This is because the recovery of failure takes up an extremely large amount of resources in dedicated backup ONUs and wireless routers. In an extreme case, the wireless routers need to reserve half of the capacity of one network, which must limit the scalability of the network and capacity. In recent years, the survivability scheme based on the mmWave technique [29] has been reported to protect the feeder segment of a TDM optical network based on the tree topology (there are a total of 64 ONUs in this network). However, such solutions have not been verified for application in protecting the feeder segment of a WDM network with a large number of users. Another limit is that although some survivable routing-based algorithms [24], [25] have been proposed, more than 5 milliseconds of multiple-hop delay still exists, and this can severely deteriorate the delay performance when the network operates in a high-load status [47].

Moreover, the approaches [9]–[13], [33] and [48] introduce extra fiber or components to achieve the protection of the distribution segment. However, whether the approach is based on the principle of wavelength routing properties or power sharing, there are common imperfections of unfair failure risk sharing for each group of ONUs or an extremely high cost for deployment of extra fiber. The average cost per kilometer of deploying fiber duct is $60,000, including the cost of the civil work and the cost of the fiber [4]. In our scheme, we design an OSM and make it cooperate with the dual-fiber ring architecture to protect the feeder segment. For the protection of the distribution segment, we set two ONUs belonging to adjacent RNs for each ONU as protective ONUs to recover the affected traffic by utilizing established microwave connectivity when a distribution-fiber fault occurs. This scheme can achieve network reliability of more than 99.9999%, which is superior to that of some existing schemes [9], [10], [12], [13], [15], [33], [40], [48]. Furthermore, in contrast to [11], [16], [30] and [34], the proposed scheme can support protection from more types

of faults, including single-fiber faults, dual-fiber faults and multifiber faults. For instance, in [11] and [30], the network will not work when there are two fibers broken in the feeder segment. In addition, in [16] and [34], if two faults occur in the ring section of the network, all the nodes located between the two positions of the faults will not communicate with the CO. On the other hand, in our scheme, since the additional construction cost for the protection of the feeder segment is shared by the large number of users of the overall network [17], the optical protection approach adopted in this segment can greatly enhance the reliability performance while not needing to introduce a high extra cost for each subscriber. Moreover, the cost of establishing microwave connectivity and its yearly spectrum leasing fee are only around $150 and $200, respectively [30], which is much cheaper than the pure optical protection approach. Therefore, the proposed scheme can not only provide more reliable performance but also possesses the feature of cost-effectiveness.

Even in comparison to [30] based on the same category of method in this paper, the proposed protection mechanisms also possesses many prominent advantages and differences, which are as follows: First, the scheme of the convergence of optical and wireless access is designed and cooperates with the proposed protection mechanisms. In this way, not only can wireless and wired service be provided in the same ONU but also the recovery of faults can be achieved by using the existing infrastructures supporting wireless service when operating in distribution-fiber fault scenarios. Hence, the subscribers have no need to pay extra construction costs for the protection of the distribution segment. Second, the RoF transmission scheme based on OCS is adopted to implement the cotransmission of radio signals and the baseband signal. In other words, the radio signals can be directly detected by the PD without the operation of up-conversion, which avoids the usage of an up-converter in each ONU and thus reduces the additional construction cost of each ONU. Third, the design of the proposed scheme is based on a dual-ring architecture, which can cooperate with the OSM to resist more types of the aforementioned failures while supporting higher scalability compared with schemes based on the tree topology [9]–[11], [29], [30]. As given in the analysis in section V.B and section V.C, by employing a certain number of EDFAs in the network to compensate for a power loss, the network scale can become very large while maintaining a relatively high-reliability performance. In addition, taking the number of ports of the AWG as 512 at present [49] as an estimation, the total number of users supported by this network will be $n\times512$. The total number of users is large, and thus the expenditure cost of each user is low.

In some pervious protection schemes [11], [13], [16], the colorless ONU structure based on the RSOA is adopted to reduce the construction cost of the ONU and enhance the wavelength efficiency. In general, in a network with reflective ONUs, the RB noise is the dominant impairment that degrades the crosstalk-to-signal ratio of the upstream transmission. However, these schemes not only do not consider the mitigation of RB noise but also do not do any work to optimize the upstream transmission performance. In our scheme, the developed OSM can cooperate with the dual-ring architecture to migrate RB noise except in the situation that an inner-fiber fault occurs. Moreover, we configure the corresponding parameters of the RSOA and obtained the optimal bias current to further improve the upstream transmission performance.

The OSM is developed based on existing commercial components, and its corresponding realistic parameters measured in the experiment are applied to analyze the feasibility of the network in terms of the network scale, network reliability, optical transmission performance and QoS metrics. In contrast to some previous studies, the feasibility of this scheme is more comprehensively and effectively verified. For example, in one such study [12], the protection scheme is based on a pair of complex 4×3 OSs, which can exchange the direction in which the signals flow and switch which signals propagate in the outer fiber or inner fiber to resist various faults. In another study [15], when a fault occurs on the inner fiber between two adjacent flexible expansion nodes, OS2 will change the operating status and make the upstream signals and the downstream signals couple from port 1 and port 3 to port 2, respectively. However, the realization of the above functions should depend on a specifically designed OSM; a relevant scheme is not mentioned in these studies. Furthermore, these studies only take the insertion loss of one ordinary OS into consideration in the simulation and do not consider the impact of other performance indicators on the feasibility of the scheme. It should be noted that some performance indicators have a significant influence on the verification of the feasibility of a scheme. For instance, the switch time of an OSM takes up most of the total network delay, and the return loss has a significant influence on the transmission performance, especially for a network with reflective ONUs based on the RSOA [19]. On the other hand, in some previous studies [11]–[13], [15], [16], [40], [48], a massive number of OSs is required to support the protection mechanisms, which will cause a potential issue of high network delay. However, these studies do not include an analysis in terms of the network delay in various fault scenarios. Of course, in our studies, although the evaluation of the QoS metrics in section V.E shows that the maximum delay will reach 57 ms in the worst case, the designed rationale of the OSM is compatible with other OSs with low switch times, such as an OS based on MEMS. Therefore, the maximum delay can be reduced to several milliseconds to satisfy the low latency requirement of future high-speed optical networks by upgrading the components of the OSM.

In conclusion, the proposed scheme possesses high reliability performance for WDM networks while also offering various advantages, including high feasibility, large scale and a relatively low cost. This study contributes to the requirement of the growing development of next-generation optical networks by developing effective protection mechanisms.

REFERENCES

[1] N. Cvijetic, M. Cvijetic, M.-F. Huang, E. Ip, Y.-K. Huang, and T. Wang, "Terabit optical access networks based on WDM-OFDMA-PON," *J. Lightw. Technol.*, vol. 30, no. 4, pp. 493–503, Feb. 15, 2012.
[2] G. Kramer, M. De Andrade, R. Roy, and P. Chowdhury, "Evolution of optical access networks: Architectures and capacity upgrades," *Proc. IEEE*, vol. 100, no. 5, pp. 1188–1196, May 2012.
[3] S. M. Lee, S. G. Mun, M. H. Kim, and C. H. Lee, "Demonstration of a long-reach DWDM-PON for consolidation of metro and access networks," *J. Lightw. Technol.*, vol. 25, no. 1, pp. 271–276, Jan. 2007.
[4] M. Mahloo, J. Chen, L. Wosinska, A. Dixit, B. Lannoo, and D. Colle, "Toward reliable hybrid WDM/TDM passive optical networks," *IEEE Commun. Mag.*, vol. 52, no. 2, pp. S14–S23, Feb. 2014.
[5] F. J. Effenberger, "PON resilience," *IEEE/OSA J. Opt. Commun. Netw.*, vol. 7, no. 3, pp. A547–A552, Mar. 2015.
[6] T. Kuri, H. Harai, N. Wada, T. Kawanishi, and M. Hosokawa, "Adaptable access system: Pursuit of ideal future access system architecture," *IEEE Netw.*, vol. 26, no. 2, pp. 42–48, Mar./Apr. 2012.
[7] H. S. Abbas and M. A. Gregory, "The next generation of passive optical networks: A review," *J. Netw. Comput. Appl.*, vol. 67, pp. 53–74, May 2016.
[8] D. Nesset, "NG-PON2 technology and standards," *J. Lightw. Technol.*, vol. 33, no. 5, pp. 1136–1143, Mar. 1, 2015.
[9] J. Chen, L. Wosinska, M. Chughtai, and M. Forzati, "Scalable passive optical network architecture for reliable service delivery," *IEEE/OSA J. Opt. Commun. Netw.*, vol. 3, no. 9, pp. 667–673, Sep. 2011.
[10] T.-K. Chan, C.-K. Chan, L.-K. Chen, and F. Tong, "A self-protected architecture for wavelength-division-multiplexed passive optical networks," *IEEE Photon. Technol. Lett.*, vol. 15, no. 11, pp. 1660–1662, Nov. 2003.
[11] Y. Chen, C. Gan, X. Li, and J. Hua, "Group protection and LAN service scheme utilizing flexible modularization and high efficiency for metro-access network," *Int. J. Commun. Syst.*, vol. 31, no. 15, p. e3783, Oct. 2018.
[12] S. Zhang, W. Ji, X. Li, K. Huang, and Z. Yan, "Efficient and reliable protection mechanism in long-reach PON," *J. Opt. Commun. Netw.*, vol. 8, no. 1, pp. 23–32, Jan. 2016.
[13] X. Li, C. Gan, K. Gou, and Y. Zhang, "A novel WDM-MAN enabling cross-regional reconfiguration and comprehensive protection based on tangent-ring," *Opt. Commun.*, vol. 430, pp. 416–427, Jan. 2019.
[14] A. Dixit, B. Lannoo, D. Colle, M. Pickavet, J. Chen, and M. Mahloo, "Efficient protection schemes for hybrid WDM/TDM passive optical networks," in *Proc. IEEE Int. Conf. Commun. (ICC)*, Ottawa, ON, Canada, Jun. 2012, pp. 6220–6224.
[15] X. Li, C. Gan, Z. Liu, H. Qiao, and Y. Yan, "Resilient intersection-ring architecture featuring online expansion and intersectional mutual protection," *IEEE J. Opt. Commun. Netw.*, vol. 10, no. 6, pp. 613–623, Jun. 2018.
[16] Q. Shao and C. Q. Gan, "High-reliable multi-wavelength optical access network expanding by a single-fiber tangent ring," *Trans. Emerg. Telecommun. Technol.*, vol. 25, no. 5, pp. 555–562, May 2014.
[17] C. Mas Machuca, L. Wosinska, and J. Chen, "Assessment methodology of protection schemes for next generation optical access networks," *Opt. Fiber Technol.*, vol. 26, pp. 82–93, Dec. 2015.
[18] E. T. Lopez, J. A. Lazaro, C. Arellano, V. Polo, and J. Prat, "Optimization of Rayleigh-limited WDM-PONs with reflective ONU by MUX positioning and optimal ONU gain," *IEEE Photon. Technol. Lett.*, vol. 22, no. 2, pp. 97–99, Jan. 15, 2010.
[19] C. Arellano, K. D. Langer, and J. Prat, "Reflections and multiple Rayleigh backscattering in WDM single-fiber loopback access networks," *J. Lightw. Technol.*, vol. 27, no. 1, pp. 12–18, Jan. 1, 2009.
[20] W. Lee, M. Y. Park, S. H. Cho, J. Lee, C. Kim, G. Jeong, and B. W. Kim, "Bidirectional WDM-PON based on gain-saturated reflective semiconductor optical amplifiers," *IEEE Photon. Technol. Lett.*, vol. 17, no. 11, pp. 2460–2462, Nov. 2005.
[21] Y. Liu, J. Wu, Y. Yu, Z. Ning, X. Wang, and K. Zhao, "Deployment of survivable fiber-wireless access for converged optical and data center networks," *Opt. Switching Netw.*, vol. 14, pp. 226–232, Aug. 2014.
[22] Y. Yu, C. Ranaweera, C. Lim, L. Guo, Y. Liu, A. Nirmalathas, and E. Wong, "Hybrid fiber-wireless network: An optimization framework for survivable deployment," *IEEE/OSA J. Opt. Commun. Netw.*, vol. 9, no. 6, pp. 466–478, Jun. 2017.
[23] Y. Yu, C. Ranaweera, C. Lim, E. Wong, L. Guo, Y. Liu, and A. Nirmalathas, "Optimization and deployment of survivable fiber-wireless (FiWi) access networks with integrated small cell and WiFi," in *Proc. IEEE Int. Conf. Ubiquitous Wireless Broadband (ICUWB)*, Montreal, QC, Canada, Oct. 2015.
[24] H. Zhang, R. Wang, H. Wang, and G. Wu, "A new lossless fault-tolerance mechanism in hybrid wireless-optical broadband access network," *IEEE Access*, vol. 6, pp. 19427–19440, 2018.
[25] L. Guo and L. M. Li, "A novel survivable routing algorithm with partial shared-risk link groups (SRLG)-disjoint protection based on differentiated reliability constraints in WDM optical mesh networks," *J. Lightw. Technol.*, vol. 25, no. 6, pp. 1410–1415, Jun. 2007.
[26] H. Sun, G. Shou, Y. Hu, and Z. Guo, "Survivability analysis of wireless bypass-based protection for passive optical network," in *Proc. IEEE 14th Int. Conf. Commun. Technol.*, Chengdu, China, Nov. 2012, pp. 88–92.
[27] K. Seppanen, J. Kilpi, J. Paananen, T. Suihko, P. Wainio, and J. Kapanen, "Multipath routing for mmWave WMN backhaul," in *Proc. IEEE Int. Conf. Commun. Workshops (ICC)*, Kuala Lumpur, Malaysia, May 2016, pp. 246–253.
[28] Y. H. Chiang and W. J. Liao, "Mw-HierBack: A cost-effective and robust millimeter wave hierarchical backhaul solution for HetNets," *IEEE Trans. Mobile Comput.*, vol. 16, no. 12, pp. 3445–3458, Dec. 2017.
[29] I. Aldaya, C. Del-Valle-Soto, G. Campuzano, E. Giacoumidis, R. González, and G. Castañón, "Photonic millimeter-wave bridge for multi-Gbps passive optical networks," *Phys. Commun.*, vol. 28, pp. 138–146, Jun. 2018.
[30] Y. Yang, K. W. Sung, L. Wosinska, and J. Chen, "Hybrid fiber and microwave protection for mobile backhauling," *IEEE/OSA J. Opt. Commun. Netw.*, vol. 6, no. 10, pp. 869–878, Oct. 2014.
[31] R. Q. Shaddad, A. B. Mohammad, S. A. Al-Gailani, A. M. Al-Hetar, and M. A. Elmagzoub, "A survey on access technologies for broadband optical and wireless networks," *J. Netw. Comput. Appl.*, vol. 41, pp. 459–472, May 2014.
[32] G. K. Chang, A. Chowdhury, Z. Jia, H.-C. Chien, M.-F. Huang, J. Yu, and G. Ellinas, "Key technologies of WDM-PON for future converged optical broadband access networks [Invited]," *IEEE/OSA J. Opt. Commun. Netw.*, vol. 1, no. 4, pp. C35–C50, Sep. 2009.
[33] E. Wong, E. Grigoreva, L. Wosinska, and C. M. Machuca, "Enhancing the survivability and power savings of 5G transport networks based on DWDM rings," *IEEE/OSA J. Opt. Commun. Netw.*, vol. 9, no. 9, pp. D74–D85, Sep. 2017.
[34] C. Y. Li, C. H. Chang, and D. Y. Lu, "Full-duplex self-recovery optical fibre transport system based on a passive single-line bidirectional optical add/drop multiplexer," *IEEE Photon. J.*, vol. 12, no. 5, Oct. 2020, Art. no. 7202310.
[35] X. Lin and J. G. Andrews, "Connectivity of millimeter wave networks with multi-hop relaying," *IEEE Wireless Commun. Lett.*, vol. 4, no. 2, pp. 209–212, Apr. 2015.
[36] K. Belbase, C. Tellambura, and H. Jiang, "Coverage, capacity, and error rate analysis of multi-hop millimeter-wave decode and forward relaying," *IEEE Access*, vol. 7, pp. 69638–69656, 2019.
[37] Z. He, S. Mao, and T. S. Rappaport, "On link scheduling under blockage and interference in 60-GHz ad hoc networks," *IEEE Access*, vol. 3, pp. 1437–1449, 2015.
[38] W. Chang, C.-W. Wu, and Y.-X. Lin, "Efficient time-slot adjustment and packet-scheduling algorithm for full-duplex multi-hop relay-assisted mmWave networks," *IEEE Access*, vol. 6, pp. 39273–39286, 2018.
[39] J. Yu, Z. Jia, L. Yi, Y. Su, G.-K. Chang, and T. Wang, "Optical millimeter-wave generation or up-conversion using external modulators," *IEEE Photon. Technol. Lett.*, vol. 18, no. 1, pp. 265–267, Jan. 1, 2006.
[40] X. Li, C. Gan, Y. Chen, H. Qiao, and Y. Yan, "Dual-fiber-ring architecture supporting discretionary Peer-to-Peer intra-communication and bidirectional inter-communication in metro-access network," *IEEE Access*, vol. 7, pp. 52360–52370, 2019.
[41] Y. Gong, C. Gan, C. Wu, and R. Wang, "Novel cobweb-topology WDM access network architecture featuring ultra-high reliability and easy scalability," *Opt. Quantum Electron.*, vol. 46, no. 8, pp. 999–1019, Aug. 2014.
[42] M. J. Connelly, "Wideband semiconductor optical amplifier steady-state numerical model," *IEEE J. Quantum Electron.*, vol. 37, no. 3, pp. 439–447, Mar. 2001.
[43] S. Zhang, W. Ji, X. Li, K. Huang, and R. Yin, "Precise failure location and protection mechanism in long-reach passive optical network," *J. Lightw. Technol.*, vol. 34, no. 22, pp. 5175–5182, Nov. 15, 2016.
[44] M. Abdullah and H. Fathallah, "Optical coding for next-generation survivable long-reach passive optical networks," *IEEE/OSA J. Opt. Commun. Netw.*, vol. 4, no. 12, pp. 1062–1074, Dec. 2012.
[45] M. S. Taqqu, W. Willinger, and R. Sherman, "Proof of a fundamental result in self-similar traffic modeling," *ACM SIGCOMM Comput. Commun. Rev.*, vol. 27, no. 2, pp. 5–23, Apr. 1997.

[46] C. H. Ji, Y. Yee, J. Choi, S. H. Kim, and J.-U. Bu, "Electromagnetic 2×2 MEMS optical switch," *IEEE J. Sel. Topics Quantum Electron.*, vol. 10, no. 3, pp. 545–550, May/Jun. 2004.
[47] S. Sarkar, H.-H. Yen, S. Dixit, and B. Mukherjee, "RADAR: Risk-and-delay aware routing algorithm in a hybrid wireless-optical broadband access network (WOBAN)," in *Proc. Conf. Opt. Fiber Commun. Nat. Fiber Optic Eng. Conf. (OFC/NFOEC)*, Anaheim, CA, USA, Mar. 2007, pp. 265–267.
[48] X. Li, C. Gan, Z. Liu, and J. Hua, "The analysis of network scale and reliability in ring-and-tree-based metro-access network with LAN service," *Fiber Integr. Opt.*, vol. 36, nos. 4–5, pp. 203–217, Sep. 2017.
[49] K. Takada, M. Abe, M. Shibata, M. Ishii, and K. Okamoto, "Low-crosstalk 10-GHz-spaced 512-channel arrayed-waveguide grating multi/demultiplexer fabricated on a 4-in wafer," *IEEE Photon. Technol. Lett.*, vol. 13, no. 11, pp. 1182–1184, Nov. 2001.

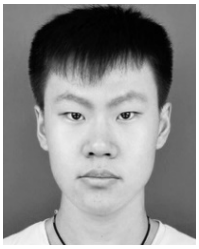

ZERUI SONG received the B.S. degree from the Department of Electronic Engineering and Information Technology, Shandong University of Science and Technology, Jinan, China, in 2018. He is currently pursuing the Ph.D. degree with the School of Information Science and Engineering, Shandong University, Qingdao, China. His research interests include novel architecture of WDM/TDM and WDM passive optical networks, design of high-speed optical communication systems, and optical sensors.

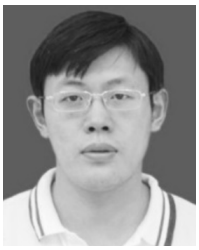

WEI JI received the M.S. degree from Beijing Institute of Technology, in 2003, and the Ph.D. degree from Beijing University of Posts and Telecommunications, in 2006. From September 2012 to September 2013, he worked as a Visiting Scholar with Queen's University, Kingston, ON, Canada. He is currently working as a Professor with Shandong University. His research interests include artificial intelligence, data center networking, and optical access networking.

RUI YIN received the B.S. and Ph.D. degrees from Zhejiang University, in 1996 and 2001, respectively. From January 2002 to December 2002, he worked as a Visiting Scholar with the Department of Physics, University of Tsukuba, Japan. From January 2003 to December 2004, he worked as a Postdoctoral Researcher and from January 2005 to December 2008, he worked as a Senior Engineer with the Institute of Materials Research and Engineering, Singapore. He is currently working as an Associate Professor with Shandong University. His research interest includes optical sensors.

JINGYAO LI received the B.S. degree from the School of Information Science and Engineering, Shandong University, Jinan, China, in 2017. He is currently pursuing the M.S. degree in optical engineering with the School of Information Science and Engineering, Shandong University, Qingdao, China. His research interests include design of tunable optical devices and optical sensors.

ZISU GONG received the B.S. degree from the School of Physics, Optical Information Science and Technology, Shandong Jianzhu University, Jinan, China, in 2015. She is currently pursuing the Ph.D. degree with the School of Information Science and Engineering, Shandong University, Qingdao, China. Her current work focuses on the microwave photonics systems. Her research interests include photonic integrated devices, microwave photonics, and radio over fiber systems.

HAO YUN received the B.S. degree from the School of Mechanical, Electrical and Information Engineering, Shandong University, Weihai, China, in 2017. He is currently pursuing the M.S. degree with the School of Information Science and Engineering, Shandong University, Qingdao, China. His current work focuses on radio over fiber and intelligent signal processing. His research interests include signal processing and wireless positioning.